AIMS Materials Science, 10(4): 652–692.
DOI: 10.3934/matersci.2023037
Received: 24 June 2023
Revised: 16 July 2023
Accepted: 22 July 2023
Published: 15 August 2023

http://www.aimspress.com/journal/Materials

Research article

Review of effective techniques for surface engineering material modification for a variety of applications

G. A. El-Awadi*

Department of Mechanical Engineering, Faculty of Engineering, Jazan University, KSA

* **Correspondence:** Email: gaberelawdi1964@gmail.com; gelawdi@jazanu.edu.sa; Tel: +966-557-448-751.

Abstract: The status of current advances in modifying surfaces for the protection of materials is reviewed in this research. The main goal of material selection is to improve and reinforce surface functionalities. A few examples of surface modification techniques include sol-gel, cladding, electroplating, plasma and thermal spraying, physical deposition of vapors (PVD), vapor chemical deposition (CVD) and beam electron physical vapor deposition (EB-PVD). Strengthening by flame, induction, laser or electron beam is one type of surface modification procedure. Other types include plasma-immersed ion implantation and ion implantation at high energies, as well as diffusion treatments like carburizing and nitriding. Friction control, improved surface corrosion and wear resistance and changes to a component's mechanical or physical qualities are all possible using surface modification methods. The study also contains contemporary research in laser therapy, PVD, EB-PVD, thermal spraying and ion implantation. Additionally, magnetron sputtering (MS) is a widely used and successful approach for thin film coating in the current study. It is crucial to remember that each approach has a distinct set of restrictions, and the method's parameters might change based on the one that is selected, such as deposition targets, overall vacuum substrate temperature, reactive or mixed gas type, pressure percentage and bias voltage, which all have impacts on the PVD technique's layer qualities. Phase formation, change in phase, hardness and film structure of monolayer and multilayer films formed on the substrate under various circumstances also cause variations in the characteristics. Additionally, ion implantation enhances the surface characteristics of layers by implanting ions such as N^+, B^+, C^+, etc. The study shows that the higher layers of multilayer enhance the degree of hardness and lower friction coefficients. To enhance the protection of thermal resistance, a thermal spraying barrier coating was coated on substrate nickel-base alloys, and the surface materials' texture, hardness

and wear rate were altered by laser beam. Additionally, a heat pipe's performance was improved by a factor of 300 by adding a tiny coating of gold.

Keywords: thermal spray; ion implantation; thermal barrier coating; laser treatment; physical vapor deposition

1. Introduction

Numerous surface protection methods have been developed recently to offer the best possible protection for substances based on their surroundings, circumstances of use and compatibility with the substrate's material. Numerous surface treatment methods exist that have been demonstrated to be efficient for protecting the surface and other functional goals and are already in use on an industrial basis. As shown in Figure 1, there are three broad categories that may be used to group all surface treatments [1,2].

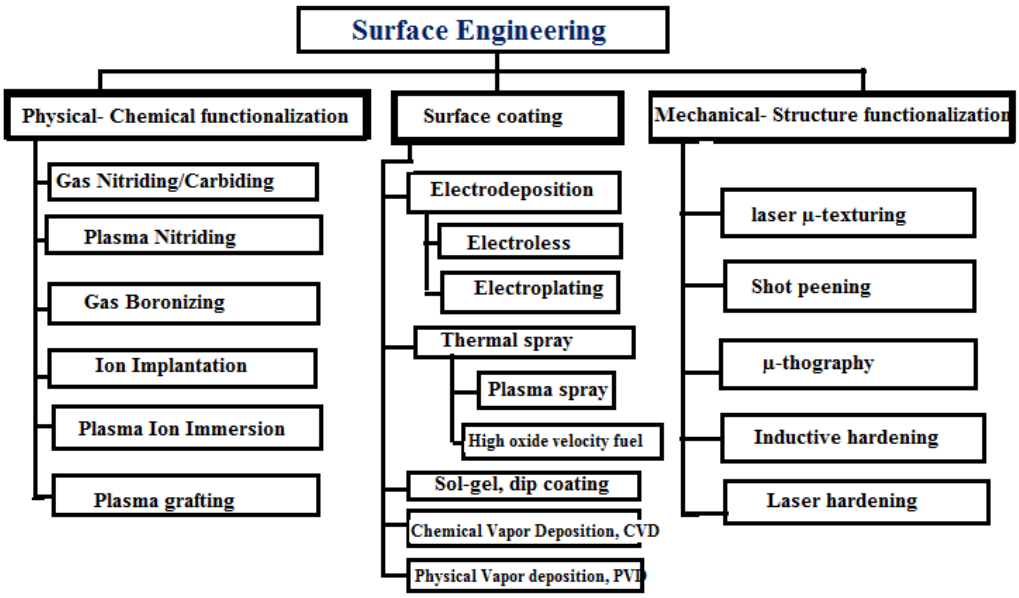

Figure 1. Classification of techniques used to modify surface [2].

1.1. Surface modification for material protection by coating technology

Understanding the fundamentals of surface characteristics and the methods used to modify them requires the use of advanced characterization techniques. Surface-related issues that come up during prototype design, modeling or process testing are easier for mechanical engineers to handle if they have a good background in surface characterization. In particular, chemical structure analysis, mechanical properties testing (such as toughness, resistance to fracture, coefficient of abrasion and wear rate), evaluation of surface topography (including roughness and texturing), thermal-chemical safeguards (such as corrosion and oxidation) and other methods of characterization are pertinent in the context of tools for manufacturing and component surface protection.

2. Materials and methods

2.1. Electro-plating and electroless coating

Due to its easy installation and top-notch performance, electro-deposition is a frequently utilized modern surface-treatment technology. With this method, metallic precursors are chemically reduced, and either self-catalytic or galvanic processes, either electroplating or electroless, are used to generate a solid, thin film on the cathode (component). In comparison to electroplating, the electroless technique has a slower rate of deposition. Figure 2 shows depositing a thin layer of metal through electroplating coating of metal using electrolytic cells onto an electrically conductive surface [3].

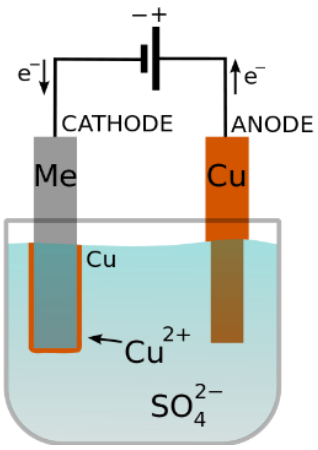

Figure 2. Electroplating cell [2].

To preserve tools and components, electro-deposition techniques frequently employ hard chrome, copper, nickel and zinc. Between CrO_3 and H_2SO_4, there is a galvanic response, which, in the absence of catalyst chemicals, results in the dissolution of metal Cr, which is how hard chromium is made. By using this method, extremely porous films that have excellent hardness and low coefficients of friction (COFs) are produced. Exceptional resistance to abrasion and extremely low stickiness are two characteristics of hard chromium. Nickel is also often used as a coating to protect tooling and component surfaces from wear and corrosion [4–6].

2.2. Chemical vapor deposition (CVD) coatings

As seen in Figure 3, chemical vapor deposition (CVD), also known as the vacuum plating technique, involves the gaseous precipitation of substrates onto a specific surface. Chemical vapor deposition, according to heat and whether there is a source of plasma, may be further separated into thermal CVD and plasma-assisted CVD (PACVD) assisting procedures. The sorts of substances that can be covered are restricted by the effects of thermal deterioration since surfaces in thermal CVD must be maintained at temperatures around 800 and 1000 °C. The tools' dimensions might change as a result of the high temperatures reached during CVD cycles.

The typical thickness of a thermal CVD coating can vary depending on the application's details, and the composition of the material that is being deposited for tooling protection might range from 5

to 20 microns. At the interfaces between the coating and the substrate, induced atomic diffusion is what gives thermal CVD coatings their excellent adhesion strength.

Thus, thermal CVD is a suggested method for tools used in cold/hot forges and metal shaping, both of which subject tools to significant normal and shear stresses. Additionally, reduced residual stresses in CVD coatings contribute to their increased toughness and resilience to fatigue. Chromium nitride (CrN), titanium nitride (TiN) and titanium nitrate with carbon (TiCN) are the three coating compounds that are most frequently employed to protect tooling. Vanadium and hafnium are two more transition metals with carbon nitrides that may be CVD-applied and provide an excellent balance of toughness and low COF. Plasma-activated CVD (PACVD), which employs plasma activating the precursor gases to encourage the formation of dense thin films, is a thermal CVD substitute. Even at deposit temperatures between 200 and 300 °C, this is still true. This reduces the consequences of steel tool size distortion. For deposition of films onto a wider range of substrate materials, PACVD is a viable substitute.

The literature also mentions other CVD activation procedures, such as microwave Radio frequency (RF) plasma-aided CVD, hollowed cathode CVD and hot-filament-aided CVD. For their high degree of hardness (1500–3000 HV) and extremely low COFs (as low as 0.1 versus bearing steels), carbon-like diamond films (CLD) are a practical alternative to protective coatings. When utilizing the proper bonding layers, they can be formed with strong adhesive strength at comparatively low temperatures of approximately 300 °C. Steel and other extremely rigid metal substrates already have silicon-based coatings pre-deposited on them to increase the adherence of CLDs to them [7–10].

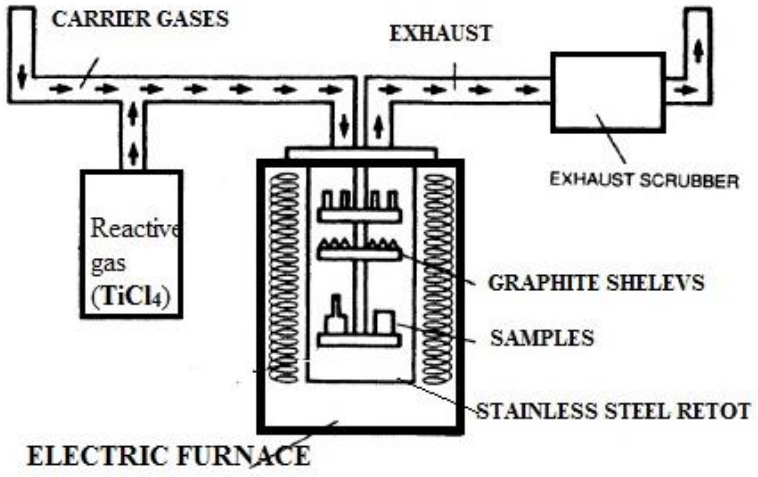

Figure 3. Schematic diagram of CVD [11].

2.3. Coatings generated via the physical vapor deposition (PVD) technique

A procedure of coating using high vacuum called physical vapor deposition is used to preserve tooling as well as for a number of technological uses, including optical science, photovoltaic conversion and decorating. PVD involves using physical techniques like arc discharge, lasers, electron bombardment-driven sputter transfer of heat, etc. to create a solid's vapor stream substance (referred to as the target) in a vacuum. Currently, the three main PVD processes utilized for industry tooling protection are electron beams (EB), magnetron sputtering (MS) and cathodic arc evaporation (CAE) [12].

2.3.1. Cathodic arc evaporation (CAE)

Cathodic arc evaporation (CAE) sources are commonly used for industrial tool protection. A target material is subjected to a high electron density in CAE, which accelerates the rate of surface evaporation. The procedure's allotted energy pushes the evaporating material. Deposition is the process through which atoms migrate toward their substrate. Energy levels are between the tens and hundreds of eV. With the intense ionization produced during electron discharges (up to 90% of the vaporized species), this technique produces homogenous, dense coatings with compressive residual strains. Reactive gases that can be introduced to the discharge process in order to deposit metal compound films include N_2, O_2 and C_2H_2, as shown in Figure 4 [13].

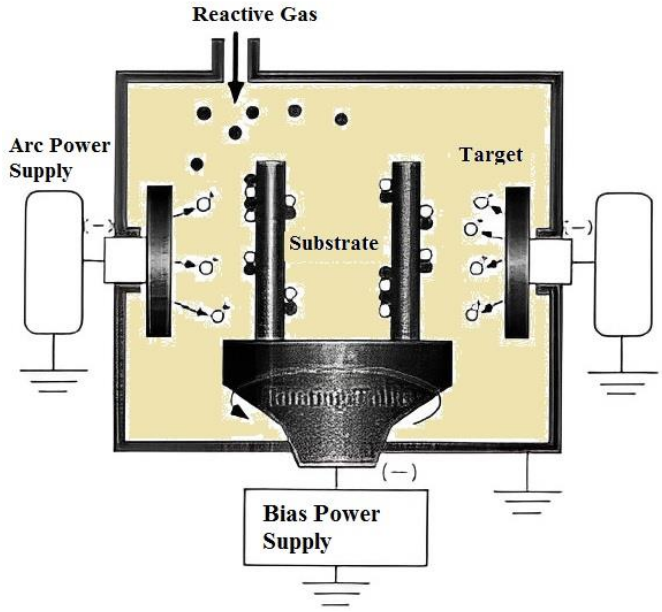

Figure 4. A schematic picture of cathodic arc evaporation (CAE) PVD [14].

2.3.2. Ion beam assisted deposition (IBAD) with magnetron sputtering (MS)

Low-pressure plasma is contained near an evaporating target by a suitable arrangement of static or cyclic electric or magnetic fields in magnetron sputtering sources. Restrictive plasma striking the subject material causes atoms to be expelled from the target material in the direction of the substrate. The sputtering atoms' energies are frequently only a few eV, and their ionization rates are typically low (less than 5% of the total sputtering atoms). Due to these factors, post-ionization and acceleration are required to give them adequate energy during the deposition phase, or impact energy. One can achieve this by applying a few tens of volts of negative voltage (also known as a bias potential) to polarize the substrate's surface. In these conditions, the ionization-inert species bombardment (often Ar atoms) onto the developing film coexists with the deposit of sputtered atoms. Each arriving atom is given enough energy by this combination technique, known as ion beam assisted deposition (IBAD), to form dense, well-adhered layers.

In order to speed up the ionization process and increase the energy of the sputtered atoms, sources of high-power impulses and magnetrons (HIPIMS) can also be utilized. HIPIMS use high-energy (MW/cm^2)

millisecond magnetic pulses. Ionization rates must reach around 80% during the sputtering operation, and all deposit species must be present. Sputtering procedures can be used to apply solid lubricants or coatings that reduce friction. All Me: C protective coatings fall under this category, where Me denotes a specific type of metal, and C denotes various carbonaceous phases that are present in the film. Additionally, low COF materials like MoS_2 or WS_2 can be deposited as thin films using sputtering techniques. (Sputtering occurs when atoms are dynamically expelled out of a target as a result of the impact of ions or energetic neutral particles.) Figure 5 displays a schematic for RF magnetron sputtering [7,15].

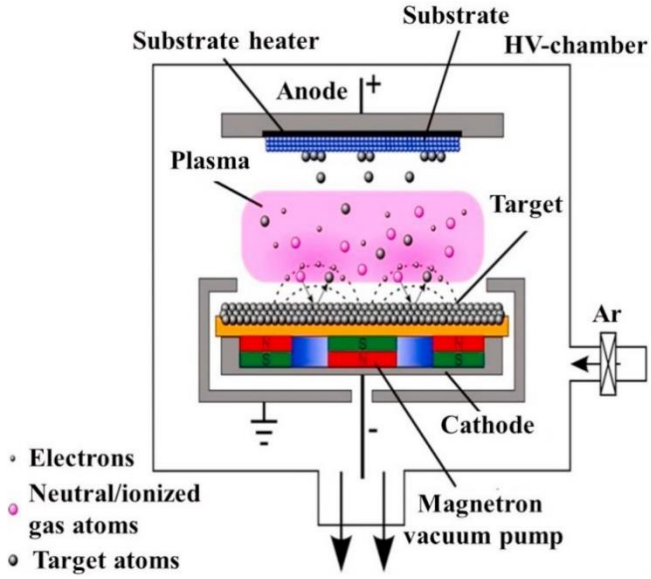

Figure 5. A schematic diagram of RF magnetron sputtering [16].

A well-known method for creating intricate and durable coatings, such as TiAlN, is reactive sputtering, and it is also known as the MSIP (magnetron sputtering ion plating) method of manufacture. Different layers can be created by adding reactive gases like oxygen, acetylene and nitrogen to the coating process. Including TiC, CrN, BN, SiC, TiCrN, TiAlN, TiAlCN, TiAlC [9], Al_2O_3 and TiAlON coatings, these coatings can enhance hardness and reduce wear, thereby extending the lifespan of cutting tools [17–20].

2.4. Thermal spray coating processes

The method of applying coatings using specialized equipment or systems that shoot molten or molten spray materials at high speeds onto a clean, ready-to-use component surface is known as thermal spray. This term, though, falls short of describing the intricate nature of the thermal spraying procedure. The fundamental concept of molten spraying is depicted in Figure 6, in which a heat source melts the covering of the basic components for the feed, which is then propelled onto a base material by process gases. Upon coming into contact with the base substance, the molten substance solidifies and forms a solid layer on top [21].

There are numerous methods used to apply the thermally sprayed coatings, including high-speed oxyfuel spraying (HVOF), spraying plasma, electric arc wire spraying and traditional spraying flame [23].

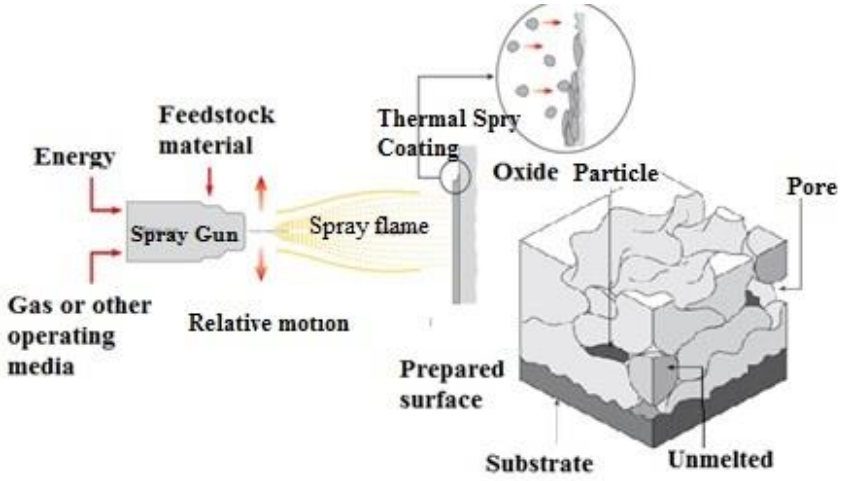

Figure 6. The presented diagram illustrates the fundamental concept of thermal spray [22].

2.4.1. Flame spray using fine particles

While the coating procedure uses spray powder rather than wires as the coating material, it functions on the same principles as the flames in the wire spray procedure (as shown in Figure 7). Since some materials cannot be made in wire shape, a larger variety of spray materials can now be used.

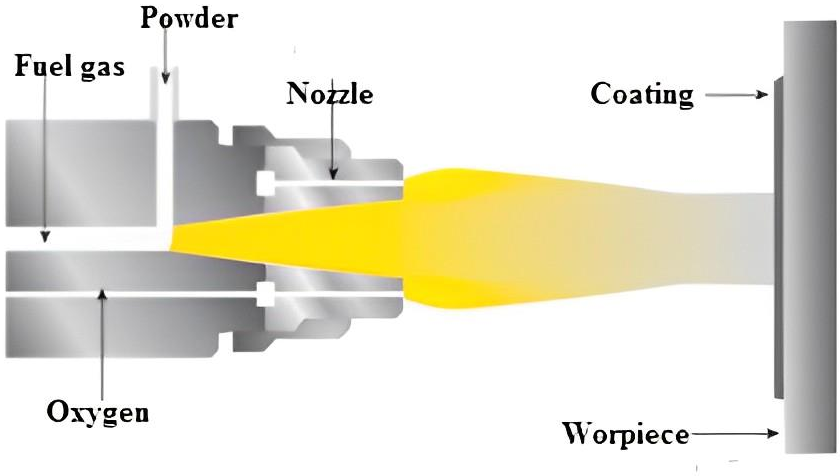

Figure 7. A diagram that demonstrates the process of powder flame spray [22].

2.4.2. Oxy-fuel spray with high velocity (HVOF)

Modern thermal spraying techniques like the fast oxyfuel spray (HVOF) process use supersonic jets as opposed to flames to spray material. Particle bombardment of the substrate occurs faster as a result, improving the coating's characteristics. In contrast to flame spraying, as depicted in Figure 8, the jet expands near the gun exit. The procedure can make use of a variety of fuel gases, such as hydrogen, acetylene, propylene, natural gas and propane, as well as fluid fuels like kerosene [22].

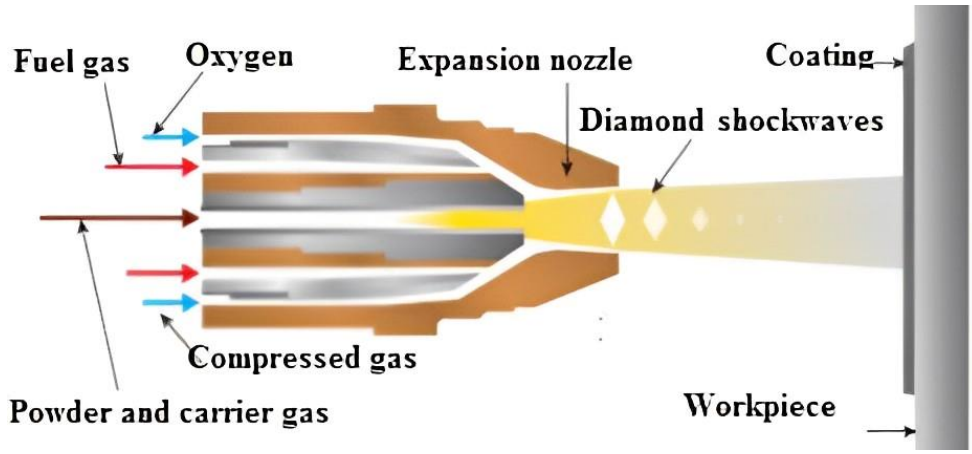

Figure 8. A diagram that depicts the process of oxyfuel spray at high velocity (HVOF) [7].

2.4.3. The plasma spraying procedure

The schematic diagram illustrates the plasma spraying principle. To start a high-frequency arc, a tungsten cathode and anode are utilized. A brightly colored plasma cloud that can reach several centimeters in length develops as the fuel, which may consist of He, H_2, N_2 or a combination of them, passes between the two electrodes and is ionized. The plume's inside can get as hot as 16000 K. The powdered spray material is introduced into the plasma cloud from outside the gun's nozzle. As depicted in Figure 9, the powder melts within the plume and is ejected onto the material's surface by gases. For some purposes, a modified form of plasma spread is used, where the coating is implemented in a regulated, lower-pressure setting. As opposed to the spraying of the atmospheric plasma technique, which applies the coating in the air, the vacuum plasma spray (VPS) produces coatings of the highest caliber because it considerably reduces the amount of oxidation that the melted particles experience [22,24].

2.4.4. Energy comparison of the thermal spray process

The general methods used by the previously stated technologies to give the spray particles thermal and kinetic energies differ. The attainable flame temperature determines the thermal energy, whereas the gas velocity determines the movement energy of the spray particle. In Figure 10, the spray techniques are compared in terms of energy, where plasma spraying's greater temperature makes it particularly appropriate for substances with high melting points, such as ceramics. The HVOF technique, on the other hand, is advantageous for spraying substances like tungsten carbide (TC) coatings due to its excellent thermal efficiency and low kinetic energy. It also has a good impact on coating qualities. A comparison of these methods is most interesting in light of the coatings produced. A comparison of coating technologies, thicknesses and applications is given in Table 1 [25].

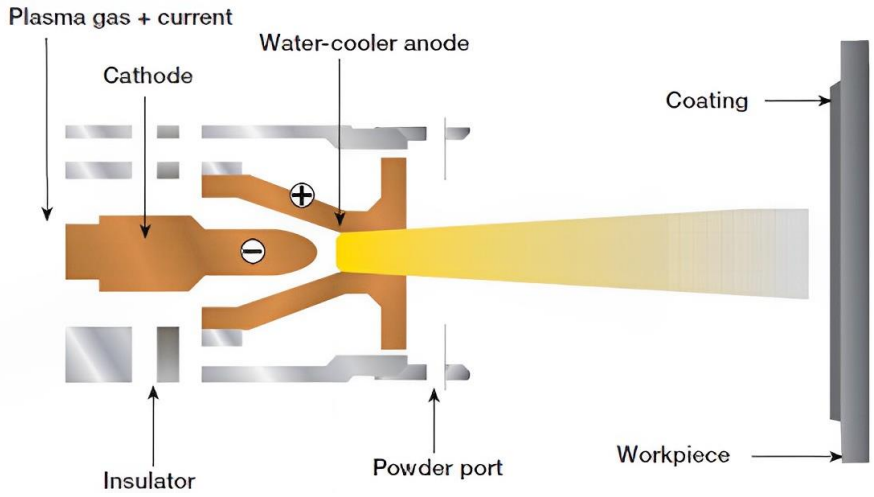

Figure 9. A schematic graphic is used to explain the plasma spray procedure [7,24].

2.5. Materials for PVD coating surface modification

TiN, TiCN, AlTiN and CrN are the PVD coatings that are most frequently employed in industrial anti-wear applications, according to Table 1. These coatings are applied between 450 and 550 °C for processing when precursor gases like O_2, N_2 or C_2H_2 are present. The temperature ranges used for tool steels, such as HSS and cold- and hot-work steels, among others, are often compatible with these deposition temperatures. Steels used in powder metallurgy for tools work particularly well for sustaining PVD-hard coatings. Likewise, cutting tools made of sintered hard metals have great load stability and adhesion strength for PVD hard coating. Among these, the coating that is most frequently used for cutting and shaping tools is titanium nitride (TiN) because of its low frictional resistance, high hardness and durability [27].

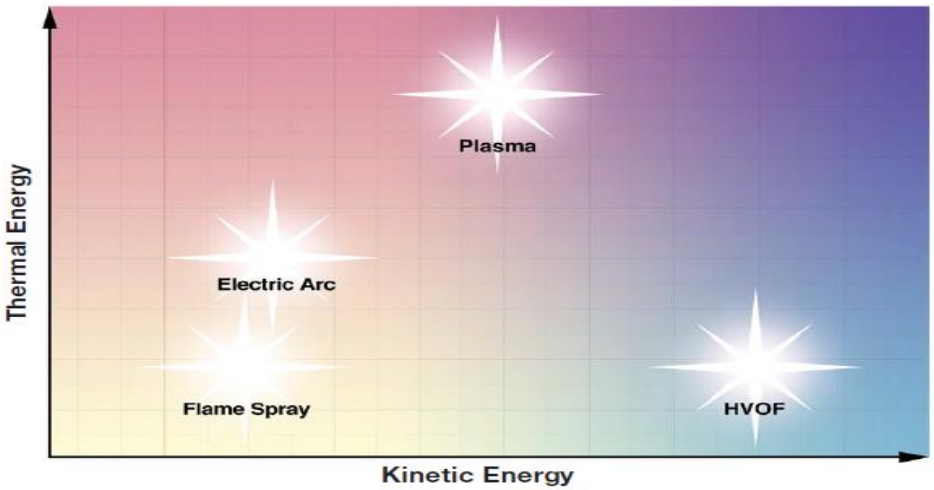

Figure 10. Energy comparison of thermal spray processes [25].

Table 1. Comparison between coating processes, materials and applications [26].

Process Coating	Thickness of Coating	Material Coating	Purpose	Application
PVD	1 to 5 μm	Ti (N, C)	Anti-wear	Machine tools
CVD	1 to 50 μm	SiC	Anti-wear	Fiber coatings
Baked polymers	1 to 10 μm		Anti-corrosion, appearance	Automotive
Thermal spray	0.04 to 3 mm	Metallic and ceramic alloy	Anti-wear and corrosion	Bearing
Plate of hard chromium	10 to 100 μm	Chrome	Anti-wear	Wheels
Overlay weld	0.5 to 5 mm	Satellite and steel	Anti-wear	Piston
Galvanize	1 to 5 μm	Zinc	Protection, anti-corrosion	Sheet of steel
Overlay braze	10 to 100 μm	Ni, B, Cr and Si alloys	Extremely dense, hard surface	Round shafts

TiN is also a good film for both decorating and protecting domestic products and other consumer products due to its golden-like tint. In contrast, TiCN has a smaller COF and a harder surface than TiN but less thermal stability. However, AlTiN coatings are now commonly used for high speed and dry-machining tools because of their higher thermal stability and better hardness than TiN. They were first developed for industrial use in the 1990s. CrN can be used in injection molding of plastic and other forming processes where galls need to be eliminated, even though it has less hardness than TiN and a far lower adhesive COF. When slipping on stainless steel, newly developed CrCN coatings demonstrate an even lower adhesion coefficient of friction than CrN. Similar to CrN in hardness, ZrN has a moderate affinity for aluminum. Due to its properties, including its low affinity for aluminum and its suitability for machining non-ferrous alloys, ZrN is advised as a coating for Al-transformation dies (extrusion, injection). Like TiN, ZrN has a brass-like hue that makes it a good candidate for decorative coatings. On bearing components that are not exposed to extremely high temperatures, solid lubricious coatings such as WC-C or MoS_2 are also used.

For a PVD coating (duplex procedures), an effective load-support surface can be created by a strong nitrided layer created utilizing nitriding procedures. With an initial thickness of two layers from 10 to 15 nm and making both of different materials, typically metal-ceramic or hard ceramic-ceramic, proposed nanometer-level thin films have been shown to display high hardness or toughness. Finely grained coverings known as nano-composites can be produced by the thin-film depositing of immiscible phases. It has been discovered that multi-phase coatings have higher hardness and toughness values than their single-phase counterparts. For instance, adding silicon to TiN or AlTiN films in amounts of around 8% to 10% can raise the hardness values of those materials by a ratio of 1.5 to 2. Furthermore, nanocomposites of (Si, Al) TiN are suitable for high-speed dry cutting of materials that are challenging to manufacture because they can maintain their mechanical characteristics even at temperatures for annealing above 800–900 °C. The many kinds of layers of coating and their characteristics are summarized in Table 2 [10,28–30].

Table 2. Common PVD coating materials' characteristics and deposition parameters[31].

Coating	PVD Process			Hardness measurements (GPa)	μ	Max. working T (°C)
	Cathodic	EB	MS			
TiN	✓	✓	✓	20–25	0.6–0.8	500
TiCN	✓	✓	✓	25–30	0.3–0.5	300
TiAlN	✓	✓	✓	25–30	0.6–0.8	500–700
AlTiN	✓	✓	✓	30–35	0.6–0.8	600–800
AlSiN-Nc	✓		✓	35–40	0.6–0.8	800–1000
CrN	✓	✓	✓	18–20	0.6–0.8	600–800
ZrN	✓		✓	25–28	0.5–0.7	400–500
WC/C			✓	10–15	0.2–0.4	200–250
MoS_2			✓	10–15	0.1–0.3	200–300
DLC			✓	10–40	0.1– 0.2	200–300

2.6. Thermal spraying coating materials

It is widely accepted that, for a thermal spray coating material, any substance that does not break down after melting is acceptable. According to the thermal spraying procedure, the coating material may take the shape of wire or powder. The most popular material classes are included in Table 3, along with their usual applications, traits and examples of how they are typically utilized. It takes expert understanding of the service environments and the raw materials involved to choose an appropriate material for coating for a certain application.

The method of manufacture of the powdered substance (i.e., agglomerated, sintered or composited), particle shape, particle size distribution and physical properties like coefficient of elongation, melting point, density and heat conductivity can all affect coating performance. There are many possible combinations because the majority of spraying materials are available as alloys or mixes. Making the right choice requires extensive knowledge and years of experience. By material class, Table 3 lists a few significant coating features [25,32].

Table 3. Classes of thermal spraying materials [33].

Material Class	Typical Alloy	Characteristics	Example
Pure metal	Zn	Corrosion-resistant	Steel construction
Self-fluxing alloys	FeNiBSi	High hardness with little porosity fused	Shafts and bearings
Alloy steel	Fe13Cr	Cheap, resistant to wear and corrosion	Repairing materials
MCrAlY	NiCrAlY	Anti-corrosion at high temperatures	Blades of a gas turbine
Nickel-graphite	$Ni_{25}C$	Anti-wear	Input duct for a compressor
Oxides	Al_2O_3	High hardness, oxidation resistance	Industrial textiles
Carbides	$WC1_2Co$	Resistance to wear	Round shafts

2.6.1. Some applications of surface modification by thermal spray coatings

Hard chromium plating can be substituted with pure chromium and different carbide coatings to provide corrosion and wear protection.

There are coatings for medical implants that function as bioactive hydroxyapatite coatings or biocompatible titanium coatings, which can hasten the formation of natural bone into the outer layer of the prosthesis.

The manufacturing components' surface characteristics that come into contact with the thread in textile equipment are very important. To increase fiber production, ceramic oxide coatings, often combined with a nickel bonded coat for corrosion prevention, are employed.

For a variety of purposes, including high temperatures corrosion resistance, insulation from heat, clearance control and the restoration of superalloy parts with coatings of similar composition, thermally sprayed coatings are used in gas turbines, both static and flying.

Coatings for rollers and cylinders are widely used in the printing industry's printing equipment. Several coatings have been created in cooperation with consumers in this business to fulfill their needs.

Plasma-sprayed chrome oxide coatings with extremely fine microstructures, which are subsequently laser engraved with a narrow and precise pattern, are advantageous for inking rollers.

There are uses for consumer items even though many thermal spray coatings were initially created for specialized components. For instance, ceramic coatings can shield iron sole plates from abrasion, and non-stick frying pans can have anti-stick coatings put on them.

Coatings are employed in the automotive sector not just for many small components but also for aluminum block engines. The interior of cylinder bores can be coated with wear-resistant materials using a specialized rotating plasma gun manipulator.

Rolls that can withstand high heat loads and protect themselves from molten zinc or corrosive slag attack are necessary for the steel working sector. For usage on newly developed parts and maintenance operations, a number of systems for coating have been certified.

The operating environments for rollers in the printing industry are varied and include wear, chemical damage from dyes, heat stress on heat wheels and stresses from cutting blades. These criteria have led to the development of coatings, particularly for calendar rolls that demand a high surface polish over an extended period of time.

Coatings are used in aerospace applications in addition to gas turbines, such as on the interior of combustion chambers [34,35].

Ni-Cr-Al, Ni-Cr and Ni-Al are frequently utilized as tools for repairing alloyed steels, and thermal spray coatings can be used to return components to their original dimensions.

PTFE, a polymer which is resistant to acids and bases and durable at extreme temperatures up to 400 °C, is a component in non-stick cookware coatings like the Teflon coating. There is little danger of overheating because household cooking pans typically do not reach temperatures of 300 °C [36,37].

2.7. Surface modification by implanting ions

Surface bombardment methods like ion implantation are frequently used for tribological purposes and in other fields like microelectronics, optics and biomaterials that call for certain surface functions. Using this method, ionized species that have been inserted into the initial atomic layers assault a solid surface. A target-specific vacuum chamber, an electrostatic acceleration mechanism, and an ion

production source are necessary for ion implantation. Using precursors that are transformed into the vapor phase, ions are produced physically in a discharge chamber. The two main ion implantation modes are linear acceleration mode and charge/mass selective mode. Prior to being filtered by a quadrupole magnet based on charge and mass, ions are pre-accelerated in charge/mass selection mode. After being filtered, the beam ions are post-accelerated and pointed at the target component [38].

Figure 11 depicts the mass/charge choosing pre-acceleration of the species ionized prior to their charge and mass filtration by a quadrupole magnet. This mode gives improved precision since it reduces impurities from different production steps. Because ion implantation uses a line-of-sight method, every surface that is being treated must be exposed to the ion beam directly. The method can only be used on simple surface geometries as a result. To get around this limitation, new sources of plasma-immersion ion implantation (PIII), which allow for the powerful bombardment of uneven surfaces with various ionized atom species, are being developed [39,40].

The ion beam is filtered, focused, and then post-accelerated before being directed towards the target component. The target component's chamber discharges all ionized species created during that process in that direction. When in use, as shown in Figure 11, the linear acceleration mode. As a result of the possibility that the final beam may contain contaminants from various manufacturing stages, this approach is less precise than the charge/mass selection option. Although it does not change the general appearance of sharp-edged tool characteristics.

On an industrial scale, it has been discovered that nitrogen ion implantation is the most efficient way to increase the hardness of metallurgical components. When nitrogen species, usually N_2^+ and N^+, are implanted onto the surfaces of transition metals, nitride phases are created, which boost the treated surfaces' hardness and toughness. For instance, examinations for aluminum, titanium and AISI 316 of hardness and coefficient of friction following nitrogen ion implantation reveal sizable variations. Additionally, nitrogen implantation results in crystalline lattice expansion at the treated metals' surfaces, which is seen as the emergence of new peaks of diffraction that are farther from the original lattice structure's diffraction angles. The lattice distortion, which results in high compressive stress, makes the implanted surfaces stronger and more durable.

The surface hardnesses of some alloyed steels, titanium or aluminum alloys and even some thermoplastics like polyethylene (PE) and polycarbonate (PC) can be increased by nitrogen ion implantation. Additionally, metal species like Cr, Ti or Al can be implanted into Ni alloys to boost their hardness. Furthermore, the implantation of gaseous and low-atomic-weight metals can enhance the anti-corrosion properties of particular alloys [38].

To increase the resistance to wear of current therapeutic materials, particularly for load-bearing implants like hip joints, a growing amount of interest is being exhibited in research into the creation of materials with excellent wear resistance and surface modification techniques. The following qualities should be present in the optimum materials or material combinations for hard tissue regeneration prostheses: a "biocompatible" chemical composition to prevent unfavorable tissue reactions, a superior resistance to environmental damage (corrosion) in the human body, enough strength to withstand the cyclic loading experienced by the joint, a low modulus to reduce bone desorption and high durability to wear to reduce debris generation [31].

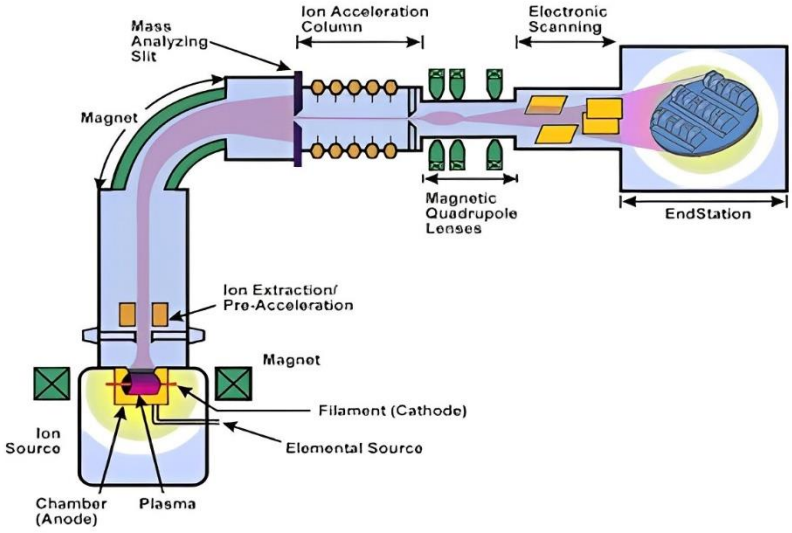

Figure 11. Schematic diagram of the implanter machine [7].

As a consequence, titanium and titanium-based alloys fall short of all "ideal" material specifications. Additionally, because people are living longer generally, and there are younger patients getting implants, biomedical research is now more focused on the constraints of the material over the long term, such as wear, strength against fatigue and long-term biological compatibility, than it is on initial implant concerns like durability, infection and short-term rejection. Technologies for surface modification are becoming more widespread as a means of tackling these growing therapeutic requirements and challenges [39].

2.8. Plasma electrolytic oxidation (PEO)

The process of anodic oxidation by spark discharge is known by various names, including ANOF, plasma electrolytic oxidation (PEO), micro-arc oxidized (MAO), anodic spark depositing (ASD), and plasma chemical oxidization (PCO) [40,41]. With the right aqueous electrolytes, it is a converter coating process for surface cleaning a variety of metallic materials that are prone to passivity. PEO was also created in the first ten years of the twenty-first century for iron-based materials, which usually exhibit undesirable passive behavior [42,43]. Metals and nonmetals that can change surfaces are of interest to many researchers in this area. The protective properties of the current coating were evident when considering structural reliability criteria, such as corrosion and tribological performances. [44,45]. Furthermore, the practical outcomes have led to the development of new applications [45,46]. This review examines the kinetics of the discharge phenomenon models and the influence of procedural variables on the process [47,48] and, consequently, on the coating qualities, such as morphology and composition, that result [49–51].

2.9. Peening applications

Several peening techniques, including traditional shot peening, ultrasound shot peening, laser shock peening and water cavitation peening, were thoroughly investigated and demonstrated to be

successful in inducing compressive residual stresses and improving fatigue durability [52,53]. Peening procedures, including peening by shot and laser treatment shock peening [54,55], are employed in order to induce residual compressive stresses on the surfaces of materials, thereby offering a safeguard against the propagation of cracks [56–58]. The aforementioned methodologies have been employed on a range of materials, encompassing hard metals that have been coated with TiCN-Al_2O_3 [59,60], high-strength steel (HSS) [61] and alloys of aluminum such as Al 2024 [62,63]. Empirical investigations have provided evidence that partial surface peening demonstrates significant effectiveness in reducing the rate of fatigue crack propagation under bending fatigue loading conditions [64]. Similarly, the application of shot peening has been observed to substantially diminish the propagation rates of minor surface cracks in Al 2024 [65]. Furthermore, recent findings have revealed that the application of laser shock peening exhibits the ability to augment the fatigue durability and mitigate the rate of crack propagation in aluminum alloys [66,67]. The aforementioned findings underscore the significance of employing peening techniques as a means of introducing compressive residual stresses to enhance both the fatigue life and resistance to crack propagation across diverse materials [53].

2.10. Characterization techniques for surface materials and coatings

Understanding the fundamentals of surface characteristics and the methods used to modify them requires the use of advanced characterization techniques. Surface engineering is a field that deals with applications that arise in relation to surfaces. Mechanical engineers can handle prototype design, modeling or process testing more easily if they have experience with surface characterization. Analyzing chemical formulas, testing mechanical properties (such as coefficients of friction, hardness, toughness, fracture, wear rate, impact, scratch test and XRD), assessing thermal-chemical stability (like corrosion and oxidation) and also assessing surface topography (like texture and roughness) are characterization techniques that are pertinent in the context of tools for manufacturing and component surface protection, as shown in Figure 12 [68–71].

3. Results and discussion

3.1. Surface modification by ion implantations

The primary objective of this study was to investigate the impact of nitrogen ion (N^+) presence on the wear resistance of a WC/Co compound. At ion concentrations of 10^{17} and 2×10^{17} ions per cm^2, low-energy N^+ ions (20 and 30 keV) blasted the WC-Co samples. Tribological tests were compared to a 100Cr6 pin that is cylindrical using four different sample types, water lubrication and Co binder concentrations ranging from 6.5% to 25%. An analysis of the X-ray spectra showed that implantation can convert the virgin surface's original (CFC) Co structure into a more resilient amorphous phase.

However, it was shown that non-implanted samples' wear properties were altered by excessively low binder content, leading to an unstable wear regime and a shift in wear rate from 0.59×10^{-7} to 2.1×10^{-7} $mm^3/(mm^2 \cdot s)$. Due to increased Co flow and the creation of oxides (Fe_2O_3, Fe_3O_4, Co_2O_3 and WO_2), SEM scans revealed that the inserted worn surface had formed a transferable layer. Cobalt flow and carbide grain extraction were used to remove the material, and the process appeared to be related to oxidation mechanisms that were aggravated by an increase in energy. The coating that was

produced, however, protected against severe abrasion. The results showed that the samples with a higher content of Co had noticeably greater wear resistance, and the sensitivity of the results to the implanted energy of N^+ ions was higher than that to dose [73–75].

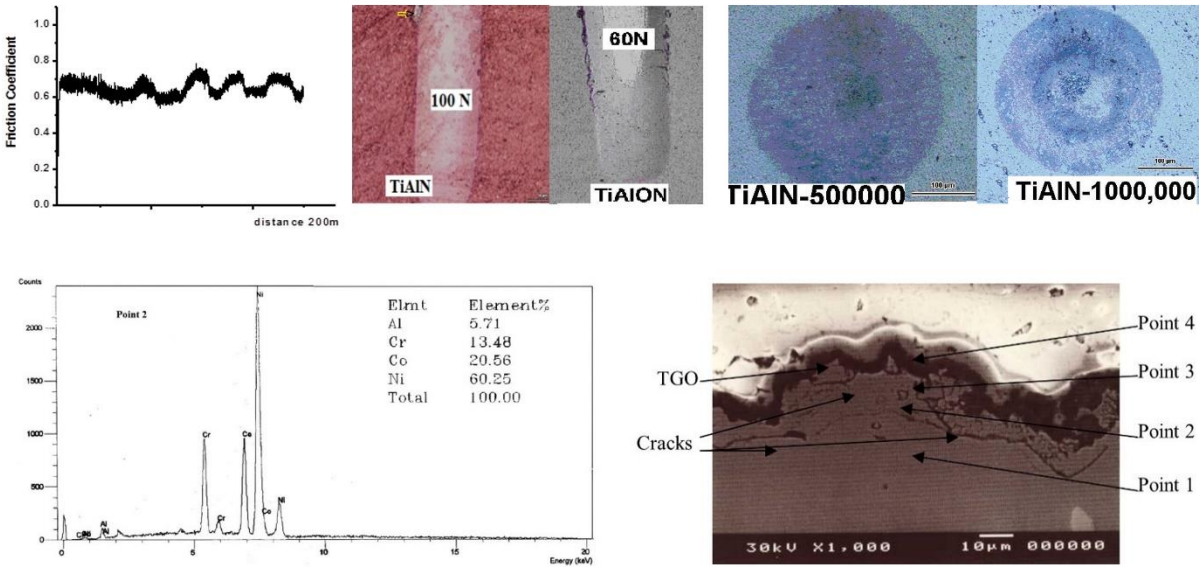

Figure 12. Some types of characterization for layers and surface evaluations: (a) friction coefficient by pin on disc measurements, (b) adhesion strength by scratch test of layers deposited by PVD, (c) impact test of layers deposited by PVD, (d) EDX analysis, (e) scanning electron microscopy (SEM) [72].

The impact of relatively low implantation energy N^+ ion implantation on the wear mechanisms of WC-Co composites was investigated. According to the study, non-implanted surfaces have a linear wear variation with Co concentration. Suddenly, a small CO content leads to an unstable wear regime and a threshold for wear rate[76].

The different energies of ion implantation of N^+, which have a significant impact on modifying wear mechanisms, promote the Co-binder phase amorphization on the newly formed surface of the implant. The primary material-removing mechanisms are the pull-out of carbide grains and cobalt flow, which are related to oxidation reactions. The GIXRD spectra of WC-25% Co are shown in Figure 13 both before and after the N^+ ion was implanted [77–81].

3.2. Surface modification by PVD coatings

Ion-sputter deposition was used to study the frictional characteristics of CrVxN coatings with varying vanadium (V) contents at high temperatures. The objective was to understand the fundamentals of coating friction behavior and examine the stick-slip phenomenon. Stick-slip test outcomes performed at slow sliding speeds were contrasted with actual contact circumstances. A novel approach that integrates coating high-temperature friction research with micro-tribology for stick-slip analysis was developed to address this issue at various scales. A friction-wear test rig is a device used to measure the amount of wear and friction between two surfaces in contact under controlled conditions ranging from 25 to 700 °C. It was used for the tribological studies.

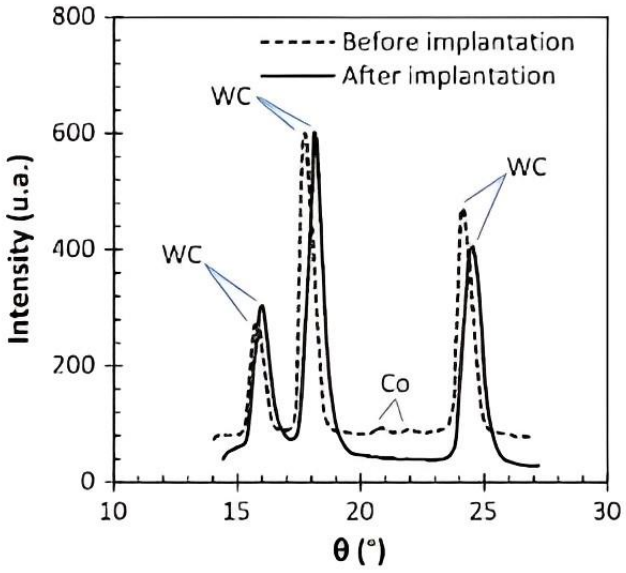

Figure 13. Pre- and post-N^+ ion implantation grazing incidence X-ray diffraction (GIXRD) spectra for WC-25% Co were obtained [76].

For tests at temperatures up to 500 °C, a novel ball-on-flat device with a heated chamber was developed to study stick-slip phenomena. It was discovered that adding up to 27–35 wt% V to CrVxN coatings improves their tribological properties by increasing their hardness, fracture resistance and grain size. Strong sticking effects were observed in friction experiments using CrVxN coatings at room temperature. High stick-slip characteristics were related to mechanical interlocking, adherence on contact sites, the surface becoming softer, a high texture and the transmission of substantial amounts of iron oxide. Low wear and slip-stick properties under frictional conditions of $V_{0.35}Cr_{0.65}N$ were observed at elevated temperatures (500–700 °C) due to the development of the V_2O_5 oxide phases with one another, making it simple to crush tribofilms at their interfaces on rubbed surfaces [82].

For CrVxN coatings with various vanadium contents, the impacts of ambient temperature effects on stick-slip, wear and pin-on-plate phenomena were investigated. SRV and stick-slip tests showed good associations with one another. At temperatures as high as 500 °C, it was discovered that adding vanadium to the CrVxN coating (up to 35%) improved its tribological characteristics and reduced friction and wear. The increased hardness, toughness and smaller particle size of the vanadium-containing CrN coatings were attributed to changes in tribological characteristics at room temperature, as shown in Figure 14. In spite of being exposed to high temperatures (500–700 °C), $V_{0.35}Cr_{0.65}N$ showed a low wear rate. When used at temperatures exceeding 600 °C, coatings with a high vanadium concentration were shown to be inappropriate [83].

Coatings of TiAlN can be created, and their characteristics can be enhanced using pulsed DC magnetron sputtering. Still, adding further substances or elements to the TiAlN coat might improve it even more. Pulse sputtering with TiAlN alterations may produce coatings that are very attractive. Table 4 summarizes the mechanical characteristics of the TiAlN coating before (as coated) and following the hardening test process up to 900 °C. These results show the performance of the coatings at higher temperatures and their potential for usage in cutting tool applications [84].

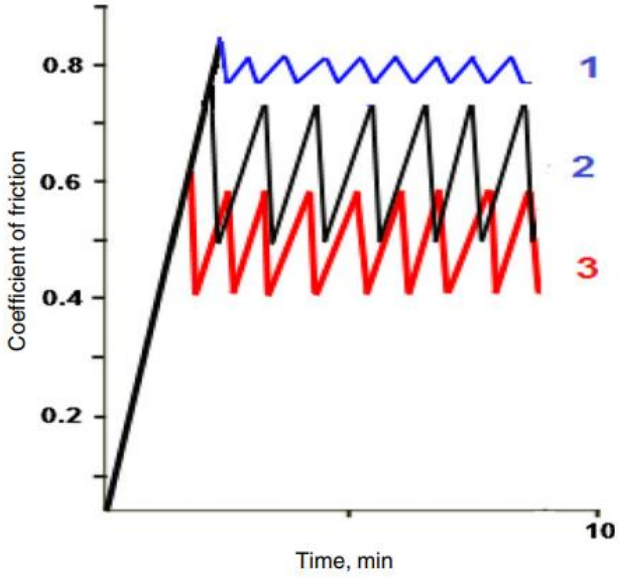

Figure 14. Friction coefficient of CrVxN [83].

Table 4. Characteristics of coated TiAlN, CrTiAlN and CrTiAlSiN [84].

Coating	Substrate bias	Layer thickness (μm)	Layer hardness (GPa)	Young's modulus as dep. (GPa)	Coating thickness (μm)	Hardness (GPa)	Y. modulus (GPa)
TiAlN	50.00	3.41	26.00	280.00	3.31	13.01	242.01
TiAlN	120.00	2.61	41.00	310.00	2.62	12.81	231.00
CrTiAlN	30.00	2.80	24.00	267.00	2.92	18.51	270.01
CrTiAlN	120.00	3.21	42.00	316.00	3.22	20.00	275.01
CrTiAlSiN	30.00	2.41	18.00	243.00	2.40	26.70	275.01
CrTiAlSiN	120.00	2.91	44.00	303.00	2.90	25.00	284.01

TiAlN-based hard and resistant-to-wear coatings were effectively deposited using the pulsed magnetron sputter method. It has been demonstrated that the TiAlN coating's shape is impacted by the addition of components such as Si and C or Si and Cr. In contrast to Si, which produced a more structureless, glass-like morphology, XRD examination showed that Cr produced a columnar coating morphology (Figure 15).

Additionally, the use of Cr improved the coating's adherence. With an indentation hardness of 40 GPa, nanocrystalline coatings with hardness values approaching the superhard area were able to be deposited using the pulsed sputter method. Furthermore, tempering experiments were carried out in an ambient atmosphere, and the findings revealed that CrTiAlN and CrTiAlSiN coatings behaved better than TiAlN coatings. Based on their claimed attributes and first-turn test results, these pulsing sputter-generated coatings show a great deal of potential for use as hard and resistant cutting tools [85,86].

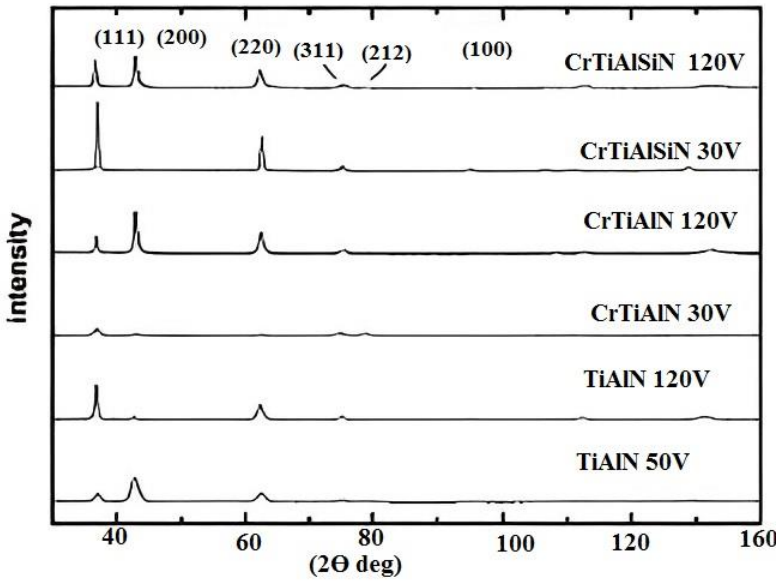

Figure 15. Different substrate bias voltages were used to study XRD on Cr, Si, TiAlN coating phases [86].

TiAlN/AlN multilayers have garnered significant interest due to their potential for modulating mechanical and tribological properties through variations in their design. This study employed TiAlN single-layer, TiAlN/AlN intermixed-multilayer, and nano-multilayer coatings produced through reactive magnetron sputtering using TiAl and Al targets. The goal was to determine how the multiple-layer design affected the coatings' thermal and tribological characteristics.

X-ray diffraction was used to examine the microstructures of the films, and XPS tests were carried out to ascertain their chemical make-up. Wear tests were used to look into the mechanical qualities, while the methods of differential thermal analysis (DTA) and thermogravimetric analysis, also known as TGA, were used to assess thermal behavior. Reactive magnetron sputtering was used to create single-layer, intermixed-multilayer and nanolayered coatings of TiAlN/AlN in a gas combination of Ar and N_2.

As can be seen in the X-ray diffractograms of Figure 16, the experimental results showed that the TiAlN single layer had a cubic structure of TiAlN with a (111) preferred orientation. Within the single TiAlN film, the respective atomic percentages were Ti 27%, Al 23%, N 48% and O 2%. The TiAlN single layer displayed brittle failure wear at 400 °C with a moderate load of 1 N applied, with wearing test grooves revealing areas where the coating was totally gone [87,88].

Through continuous deposition on rotating substrates that had both TiAl and Al targets turned on, TiAlN and AlN-i were made possible. Both substances were intermixed to form a single layer that only produced a cubic TiAlN phase, which had a larger aluminum content compared to the TiAlN sample used as a reference but a lower level of order. The total composition of the coatings' primary components was revealed by the depth profile to be Ti 19%, Al 38%, N 39% and O 4%.

In the meantime, just one target was alternately shuttered to produce multilayer TiAlN or AlN-n. The expected growth process was confirmed by the equal distribution of the XPS Al signal into the two molecules TiAlN and AlN. Al 40%, N 36%, Ti 23% and O 1% were the major components of the coatings overall, according to the depth profile. Table 5 displays the results in summary [87].

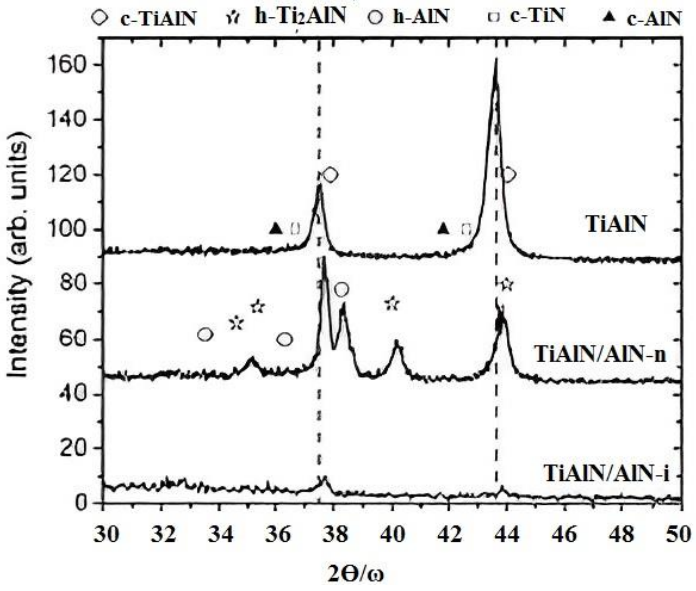

Figure 16. XRD of TiAlN multilayers TiAlN/AlN [87].

Table 5. The friction coefficient (μ), wear rate and their respective standard deviations were measured at two different temperatures, namely, 30 and 400 °C [87].

Coating layer	Temp. (°C)	Rate of wear ($mm^3/N/m$) × 10^{-6}	σ_{WR}	Friction coefficient	σ_{μ}
TiAlN	30.00	5.110	3.00	0.5601	0.0261
	400.00	8.900	2.00	0.5601	0.0241
TiAlN/AlN-n	30.00	4.420	5.00	0.5401	0.0231
	400.00	1.351	5.00	0.3301	0.0210
TiAlN/AlN-i	30.00	4.191	4.00	0.5401	0.0181
	400.00	1.421	5.00	0.5301	0.0251
WC-Co	30.00	15.81	3.00	0.6401	0.0261
	400.00	19.01	5.00	0.6601	0.0251

3.3. Surface material modification by laser

Numerous scientific fields have found use for lasers, including photographic chemistry, microscopy, lunar laser varying and nuclear fusion, in addition to fields like materials processing and spectroscopy. The coherency and monochromaticity of the laser beam, which allow it to travel in a straight path with little deviance and to be generated in a broad range of light intensities, beam types, and wavelengths, are the sources of the laser beam's versatility [79,89] by harnessing a laser's heat energy to change the material's properties, metal surfaces can be modified using laser technology. The use of a laser for processing offers a number of benefits over more traditional techniques, including localized surface heating that does not alter the properties of the substrate material or cause damage, high operational precision and speed and lower costs. Utilizing a laser's heat energy to alter the surface characteristics of a material is how laser technology is used to modify metal surfaces [90,91].

The processes include laser alloying, transformational hardening, surface amorphization, shock hardening, cladding, and glazing. Various techniques can be employed to alter the properties of laser-enabled surfaces. These approaches vary in terms of the modifications they make to the surface structure of the material and the rate of energy absorption. Laser surface processing has a number of benefits over traditional techniques for selective surface hardening, including the development of a fine-grained and uniform microstructure, minimal creation of non-equilibrium and amorphous structures, minimal thermal damage to the underlying substrate, reduced grain development and distortion and an increase in the solid solubility of alloying elements. With the bulk of the qualities remaining unchanged, these advantages can be exploited to improve mechanical properties like hardness, strength, toughness, fatigue resistance and corrosion resistance [78].

Tungsten carbide ceramic powders with 12% Co were applied using air plasma spraying to a stainless steel substrate, producing two types of coatings with different porosities and splat morphologies. After that, the samples that were coated were subjected to CO_2 laser treatment in an inert atmosphere while several tests were conducted to optimize the laser's settings. The thickness of the spray coatings had an impact on the melt depth and microscopic structures attained, as shown by the characterization of the laser-treated surfaces and their comparison to the as-sprayed surfaces. Both samples underwent laser melting, resulting in the phases Co_3W_3C, $Co_3W_9C_4$ and W, as depicted in Figures 17 and 18. Co_3W_3C, $Co_3W_9C_4$, and W phases were created during the observed increase in Co_3W_3C, $Co_3W_9C_4$ and W phases that had developed throughout the cermet layer's growth, which is why its hardness was seen to rise.

Nevertheless, air plasma spraying frequently yields cermet layers that are sprayed with flaws, including porosity and poor substrate contact. Two distinct coating types were sprayed at various standoff distances to address this (as shown in Figures 17 and 18) the comparison of coating deposited at standoff distance 80 and 100 mm showed decreased permeability, less thickness, and a superior interface. The hardness of the coating was further increased by adding tungsten carbide to the base metal. In contrast to thick coatings, thin sprayed coatings showed greater microhardness and fewer defects such as porosity and HAZ (as illustrated in Figures 19–22) [92–99].

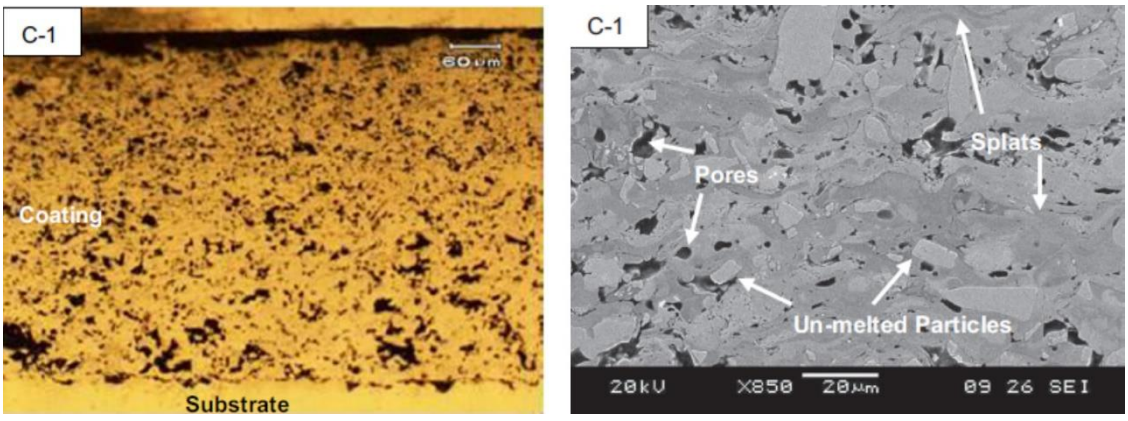

Figure 17. The thickness of the coating and its defects were evaluated for the layer sprayed at a standoff distance of 80 mm [55].

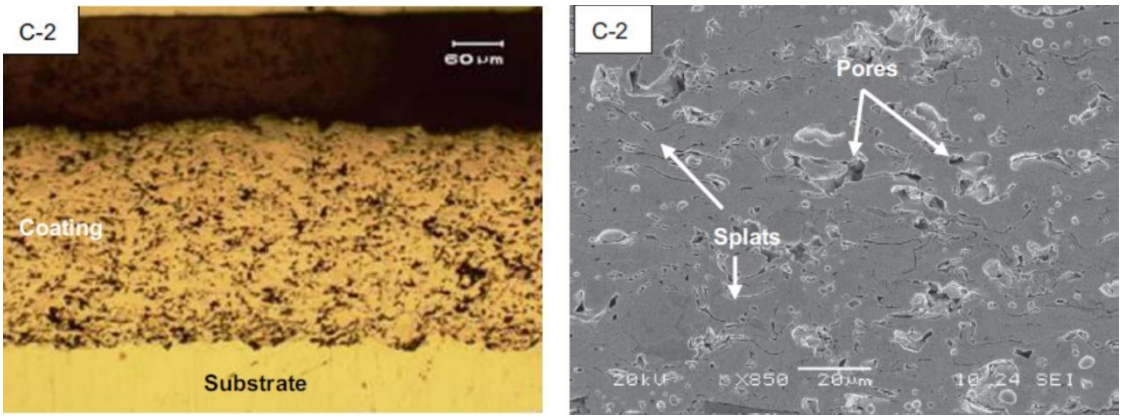

Figure 18. The thickness of the coating and its defects were assessed for the layer sprayed at a standoff distance of 100 mm[55].

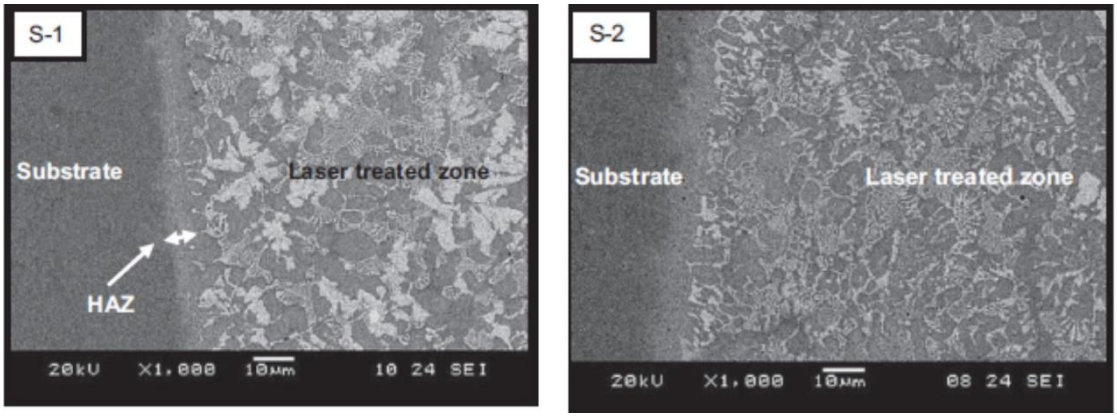

Figure 19. An analysis of the heat affected zone and interface close to the HAZ in comparison to the laser-treated location for both S-1 and S-2 samples [55].

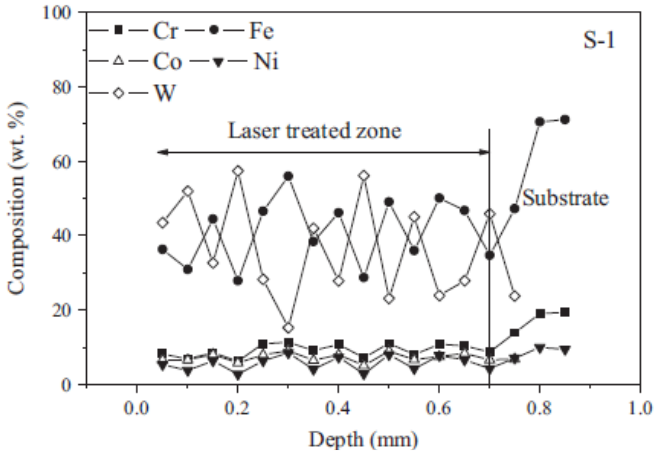

Figure 20. Analyzing the variation in composition as it relates to the S-1 sample's laser-melted zone's depth [55].

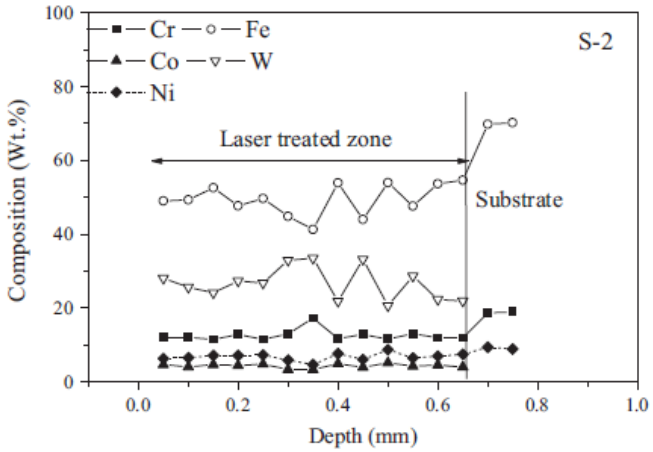

Figure 21. Investigating how the composition varies along the depth of the laser-melted zone in the S-2 sample [55].

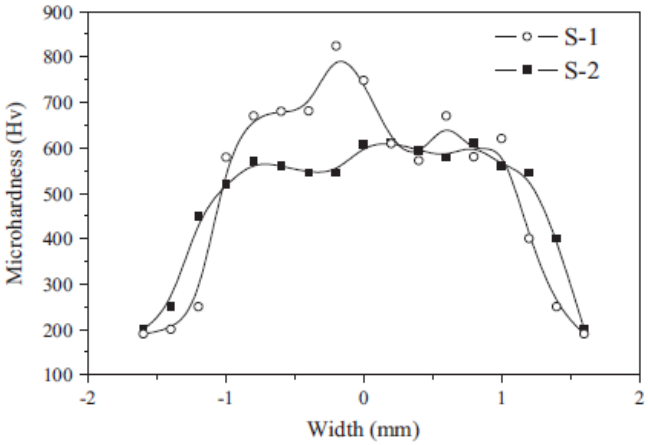

Figure 22. The microhardnesses of the S-1 and S-2 samples were compared across their cross sections [55].

The coatings passed through melting by the pulsed Nd: YAG lasers, as shown in Figure 23. In order to achieve a consistent microstructure and reduce the occurrence of surface porosity, microcracks, and partially or completely unmelted regions, plasma-sprayed Al_2O_3 with the addition of 40 wt% TiO_2 was employed, as illustrated in Figure 24. The surface microscopic structure, chemical composition, microhardness, and roughness of both the as-sprayed and laser-melted coatings were analyzed using a profilometer, X-ray diffraction, Vickers hardness, and SEM-EDX, as depicted in Figure 25. These examinations were conducted at power densities of 640 and 800 kW/cm^2.

As evidenced by the inclusion of a stable Al_2O_3 phase and an Al_2TiO_5 phase with a segmented fracture network in both laser-melted coatings, the use of laser melting has improved the coating's surface uniformity. The observed results in Figure 23 indicate a reduction in average surface roughness and an increase in surface microhardness, which suggest the formation of a uniform microstructure. This phenomenon was achieved by varying the laser power density within the range of 640 to 800 kW/cm^2. These findings support the use of pulsed laser melting to improve or alter the surface characteristics of coatings made of plasma-sprayed Al_2O_3 and 40 wt% TiO_2 [98].

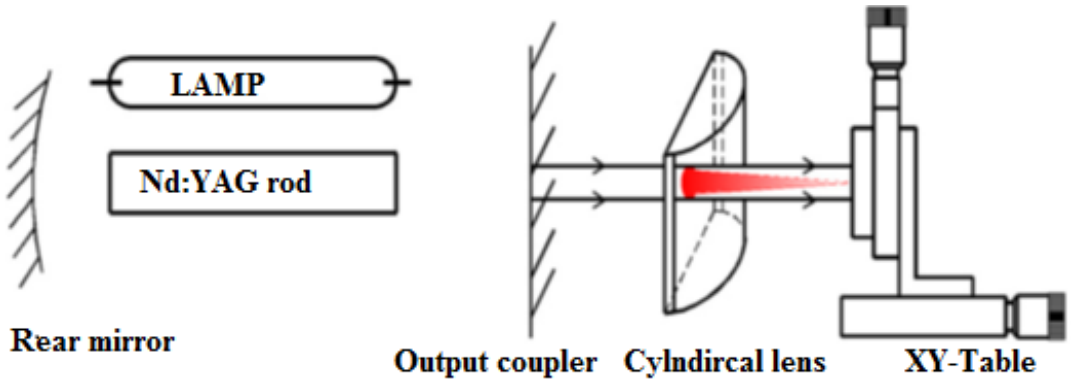

Figure 23. A diagrammatic representation illustrates the system with pulsed Nd:YAG laser [98].

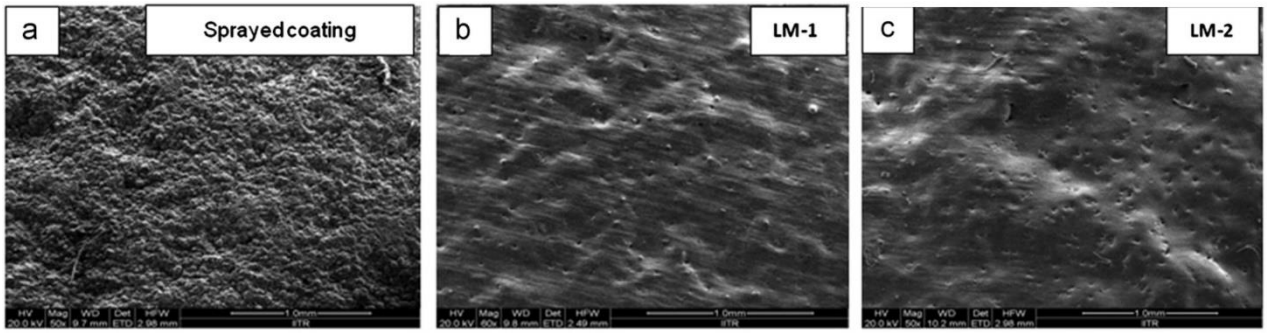

Figure 24. The exterior morphologies of A40T are displayed in (a) the spray-applied form and (b, c) the laser-melted coats of LM-1 and LM-2 [98].

A Ti6Al4V alloy's microstructure and wear properties were improved for implant applications using laser surface melting (LSM). Using input energies of 42 and 68 J/mm^2, respectively, the alloy substrate was burned at 250 and 400 W with a scan speed of 5 mm/s. The outcomes showed that the rapid cooling rates, ranging from 2.25 × 10^{-3} to 1.41 × 10^{-3} K/s during LSM, caused the substrate's equiaxed microstructure to transform into a mixture with an acicular matrix after LSM. The thickness of the remelted zone rose with increasing energy input, going from 779 to 802 to 1173 to 1199 nm. The alloy's grain size also grew from 4.8 to 154–199 nm as a result of the experiment's sluggish cooling speeds. As a result of the increased hardness brought about by LSM, the Ti6Al4V alloy had the lowest in vitro degradation rate of 3.38 × 10^{-4} mm^3/N·m compared to the unmodified substrate, which had a wear rate of 6.82 × 10^{-4} mm^3/N·m.

The results of the investigation indicated that higher cooling rates during laser melting at 250 W resulted in finer microstructural features than those at 400 W, as illustrated in Figure 26. Additionally, it was found that the Ti6Al4V alloy substrate that had been formed had an average hardness that was 15% to 22% lower than that of the melted region. When compared to the untreated substrate (6.82 × 10^{-4} mm^3/N·m), the samples treated at 250 W likewise had the lowest in vitro wear rate (3.38 × 10^{-4} mm^3/N·m), as shown in Figure 27. The improved in vitro tribological performance was most likely caused by the laser-treated materials' increased hardness and resistance to corrosion as well as layers of passive oxide production [100].

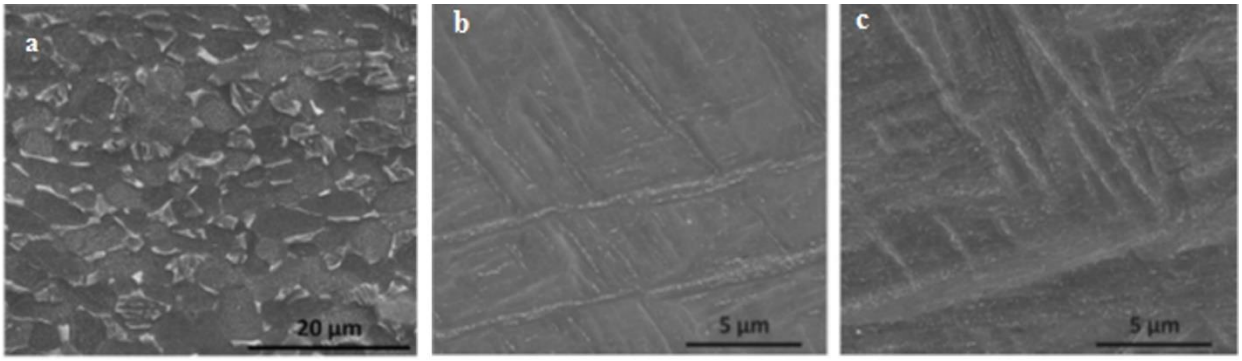

Figure 25. The microstructures of the Ti6Al4V alloy were analyzed using high magnification FESEM, including (a) the substrate in its as-received state, (b) the substrate that underwent laser melting at 250 W with 2 passes and (c) the substrate that underwent laser melting at 400 W with 2 passes [100].

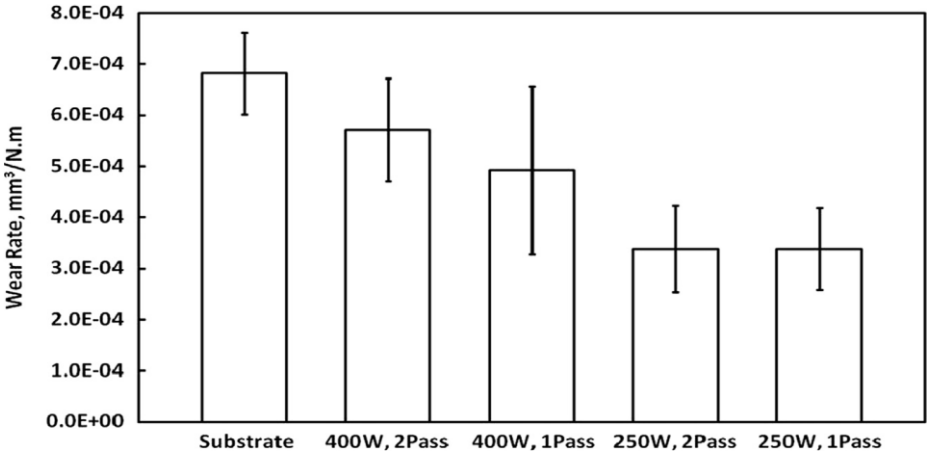

Figure 26. A comparison was conducted to evaluate the Ti6Al4V alloy in vitro wear rates with and with no laser surface melting [100].

3.4. Thermal protection as a surface modification technique for materials

3.4.1. Thermal barrier coatings as a means of thermal protection

In gas turbines or aero engines that run at high temperatures, coatings with thermal barriers (TBCs) are complex material systems that are often applied to metallic surfaces. By using thermal insulating materials to protect components from high and sustained heat loads, these coatings serve as a method of exhaust heat control. As a result, structural components are not exposed to as much heat during operation, which lowers oxidation and fatigue caused by heat and lengthens part life. In some turbine applications, coatings with thermal barriers (TBCs) for fluids functioning at temperatures greater than the metal airfoil's melting point may be possible when combined with active film cooling. There are four layers that make up a TBC: a metal base, a metal bond coating, thermally generated oxide and a ceramic topcoat. Low conductivity yttria-stabilized zirconia (YSZ), which is stable at standard operating temperatures, is typically used as the ceramic topcoat. Though they have a lower fracture toughness than YSZ, new ceramics (rare earth zirconates) have been found in recent tests to perform

better at temperatures above 1200 °C. The ceramic layer produces the TBC's biggest thermal gradient and maintains a cooler temperature in the bottom layers than the surface [101].

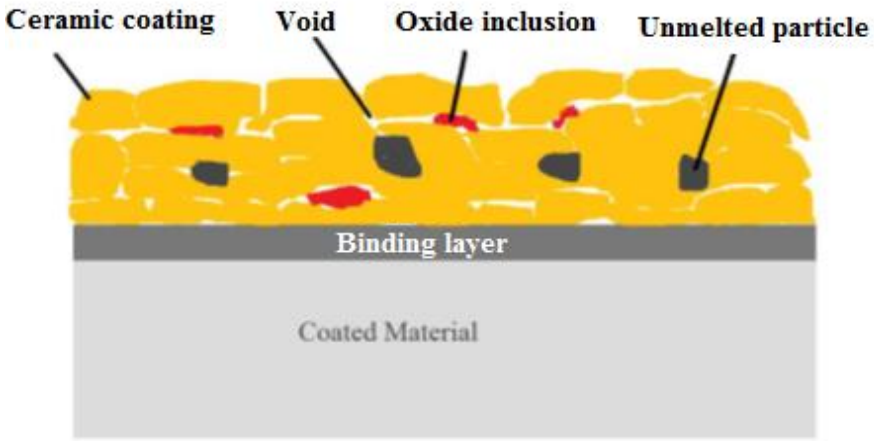

Figure 27. System for coating thermal barriers [101].

A few of the degradation modes that can cause thermal barrier coatings (TBCs) to fail include molten deposit deterioration, hot corrosion, rapid oxidation and mechanical rumpling of the bond coat under heat cycle exposure (especially in aviation engines). Thermal fatigue and substantial lifespan reduction of the metal are both caused by oxidation, which can also tear off portions of the TBC. Three types of TBC systems are commonly distinguished: graded, duplex and triplex [102].

A bonding metal film and a ceramic topcoat make up the double-coated structure of the traditional thermal barrier coating (TBC) approach. For a number of reasons, modern TBCs feature a ceramic overcoat that is separated into layers. One illustration is the double-layer system, which blends modern materials like pyrochlores or perovskites as the topcoat layers with traditional yttria-stabilized zirconia (YSZ) as the bottom layer. When compared to normal YSZ, these systems have shown greater temperature performance. The temperatures and gas pressures of modern gas turbines are higher, which results in a higher percentage of radiative heat flow. It is possible to prevent this radiation from heating up metal substrates by using coatings with increased reflectivity. Suspension plasma spraying is an efficient way to produce these coatings, which are sprayed on top of the TBC system and further enhance the coating's grade and performance [103].

Particular outputs that exceed the strength threshold of typical aluminum piston alloys have been produced as a result of the thermal loadings produced by certain diesel engine applications. A common method for improving the operational effectiveness of diesel engines' high-temperature components is the use of functionally graded coatings. Thermal barrier coatings are now being evaluated in an effort to increase component durability and provide a technique to lessen heat rejection. Thermal barrier coating systems are investigated using a finite element model that takes into account the effects of boundary conditions, residual stress, coating thickness and material properties. A transitional zone connects the metallic bond barrier to the cermet layer in the coatings mentioned above, and subsequently the cermet layer to the ceramic layer. The deposition of NiCrAl, NiCrAl + $MgZrO_3$ and $MgZrO_3$ metallic, ceramic and powdered ceramics onto the substrate was regulated by thermal studies. The numerical results of steel and AlSi-made pistons were compared and contrasted.

The findings show that both AlSi alloy and steel pistons' maximum surface temperatures significantly increased as a result of the functional graded coating, with a 28% rise for the former and a 17% increase for the latter [104–106].

To compare the temperature distributions of an aluminum alloy piston with and without a ceramic coating, a comparative analysis was done. It was discovered that covering pistons with ceramic improves their maximum surface temperature. In particular, compared to uncoated pistons, the application of a zirconia stabilized with magnesium oxide ($ZrMgO_3$) coating improved performance by about 28%, a mullite ($3Al_2O_3$-$2SiO_2$) coating improved performance by about 22%, and an alumina (Al_2O_3) coating improved performance by about 21%.

The use of a ceramic coating on an aluminum alloy piston raises the temperature in the engine's combustion chamber and improves the thermal durability of the underlying metal, according to the results of software simulations. As shown in the Ansys simulations (Figure 28), the rise in combustion chamber temperature causes the engine's thermal efficiency to increase [106–109].

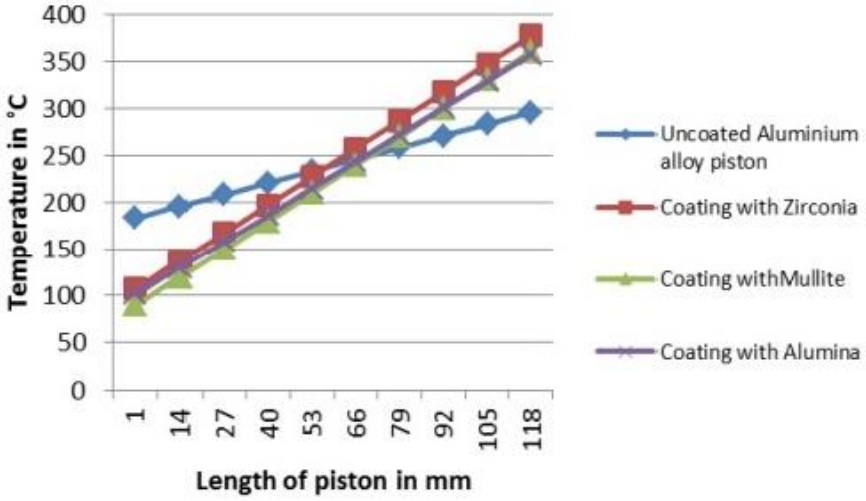

Figure 28. Simulation of thermal barrier coatings (TBCs) for piston diesel engines made of aluminum alloy using Ansys software[108].

Gadolinium zirconate ($Gd_2Zr_2O_7$, GZ) was employed in plasma spraying to generate a double-ceramic-layered (DCL) thermal barrier coating system.

The system consisted of a bottom ceramic layer composed of partially stabilized Y_2O_3 at 4.5 mol% and a toughened gadolinium zirconate ($Gd_2Zr_2O_7$) ceramic layer on top. The reaction of the DCL coating to thermal stress was examined. The fracture toughness of the matrix was improved by fortifying the GZ top ceramic layer with nanostructured 3 mol% Y_2O_3 and partially stabilized ZrO_2 (3YSZ). The single-ceramic-layered (SCL) GZ-3YSZ composite coating's resistance to thermal shock was significantly outperformed by the DCL coating in this test. Two things are thought to have contributed to this improvement: First, the incorporation of nanostructured YSZ particles boosted the fracture toughness of the top ceramic layer; and second, the use of 4.5 YSZ as the bottom ceramic layer improved stress tolerance. Additionally, the uppermost ceramic layer's comparatively poor fracture toughness and the bond coat's oxidation are principally blamed for the failures. A comparison of the DCL's surface image coatings in both their as-sprayed and thermally shocked stages is shown in Figure 29.

The coating's spallation is typically seen in a single chunk rather than gradually and unevenly, as seen in Figure 30b.

The top ceramic layer's extreme spalling and apparent tearing off are clearly visible. Furthermore, under the circumstances of thermal shock experiments, it can be seen that the crack starts near the coated specimens' periphery. The elevated stress levels present at the specimens' edges are to blame for the observed phenomena. After a thermal shock test, Figure 30 depicts the resulting microstructure of the DCL coating's spallation zone. The integrity of the bottom ceramic layer of the 4.5YSZ remains even in the spallation zone, as seen by the similar structure to the as-sprayed situation and strong adherence to the bond coat.

The thermal barrier coating (TBC) made of 4.5 mol% yttria-stabilized zirconia (YSZ) is recognized for its exceptional thermal conductivity and long cycling durability at high temperatures up to 1473 K. The superior adhesion of the 4.5 YSZ bottom ceramic layer to the bond coat was observed after conducting the study's thermal stress test. Figure 31a,b illustrates [110–112].

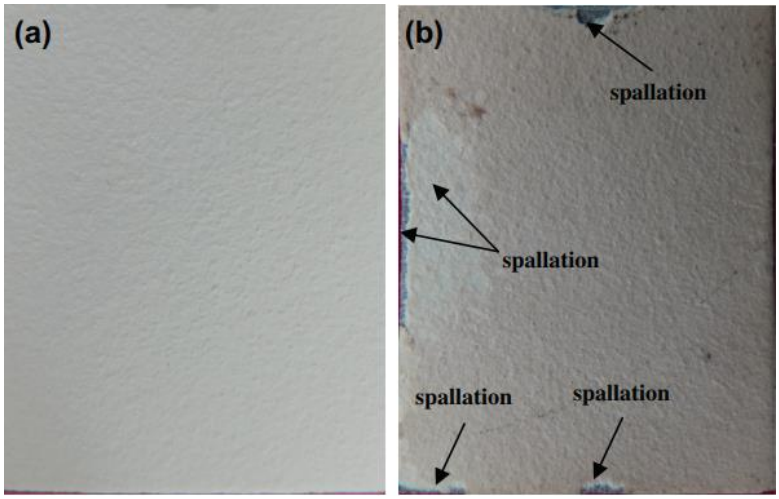

Figure 29. The DCL coating has been captured in surface photographs that depict its appearance in two different conditions: both as-sprayed and thermally shocked, (a) and (b) [112].

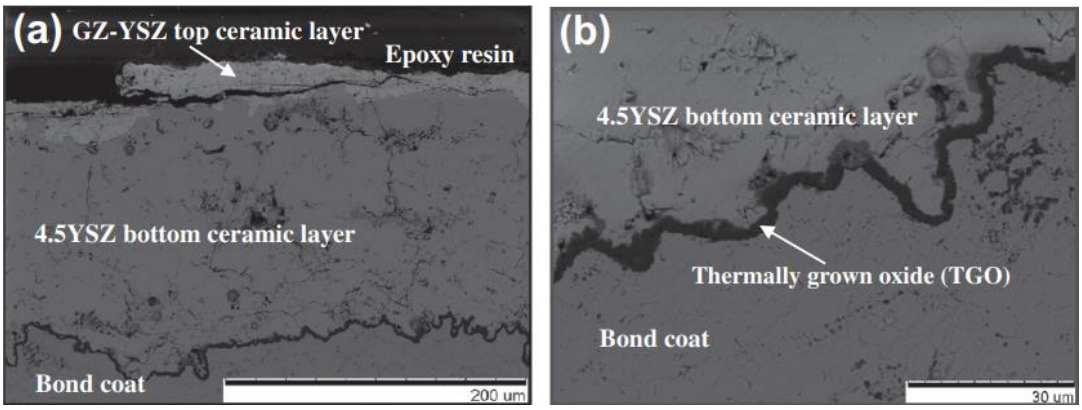

Figure 30. The DCL coating's microstructure after thermal shock is shown in cross-section [112].

According to its thermal shock cycle lifetime, which was over three times longer than that of the monolithic GZ coating and two times longer than that of the GZ-YSZ coating, the GZ-YSZ/4.5YSZ DCL coating was shown to have a significantly increased level of thermal shock resistance. NiCoCrAlY coatings have been widely produced using thermal barrier coating (TBC) systems, which use them as acceptable bond coatings thanks to physical vapor deposition electron beam (PVD-EB) or as efficient oxidation resistance coatings.

The oxidation resistance of the coatings is compromised by the inherent imperfections resulting from the EB-PVD process. The investigation illustrated in Figure 31 scrutinized the deposition of NiCoCrAlY coatings through the utilization of physical vapor deposition (PVD) technique, subsequently modified via electron beam. The elevated energy of metal ions and higher mobility of adatoms are responsible for the substructure that was detected on the new coatings' surfaces of each particle. It was observed that grains had a strongly (111)-oriented crystallographic microstructure. The coatings' endurance was demonstrated in comparison to coatings created using conventional EB-PVD, with a noticeable improvement. Furthermore, the oxidation performance at a temperature of 1373 K demonstrated that the innovative coatings possessed exceptional resistance to oxidation, as shown in Figures 32 and 33 [113–115].

According to the PA coatings have a stable grain texture with crystallography (1:1) and a terraced grain substructure. Due to the unique structural properties of the PA coating, it was found that its toughness was greatly increased when compared to the typical coating produced using EB-PVD. It was discovered that the PA coating caused a mass increase of 0.950 mg/cm^2 after the material underwent 100 hours of isothermal oxidation at 1373 K. The fact that this number was discovered to be two thirds of the mass gain seen for the EB coating suggested that the growth scale rate for the PA coating was less rapid. As shown in Figure 33, the PA coating was found to have very little spallation and Y-rich oxides. The twin structure may be able to improve the coating's ability to resist oxidation. To further understand the related mechanism, more study must be done. It is advised that cyclic oxidation tests be performed to examine the benefits brought on by the coating's enhanced toughness [115].

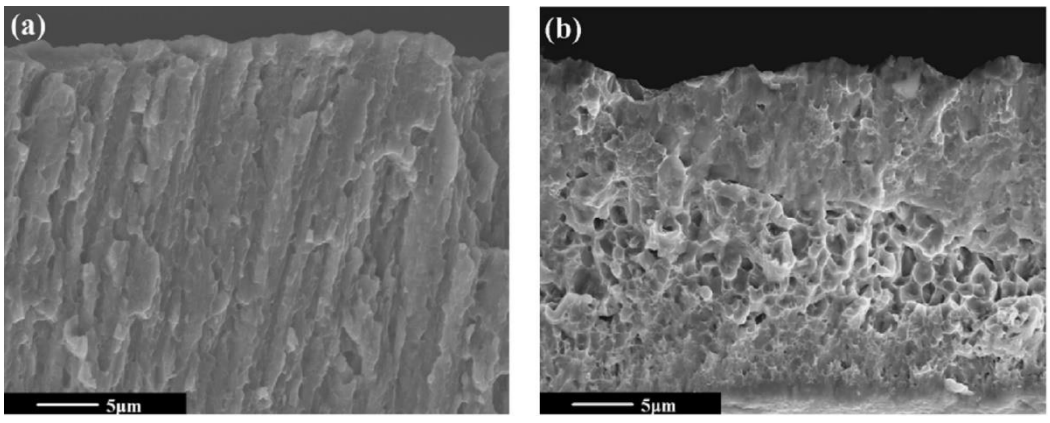

Figure 31. Examining the coatings' as-deposited fracture morphologies, (a) EBPVD, (b) PA-EBPVD [115].

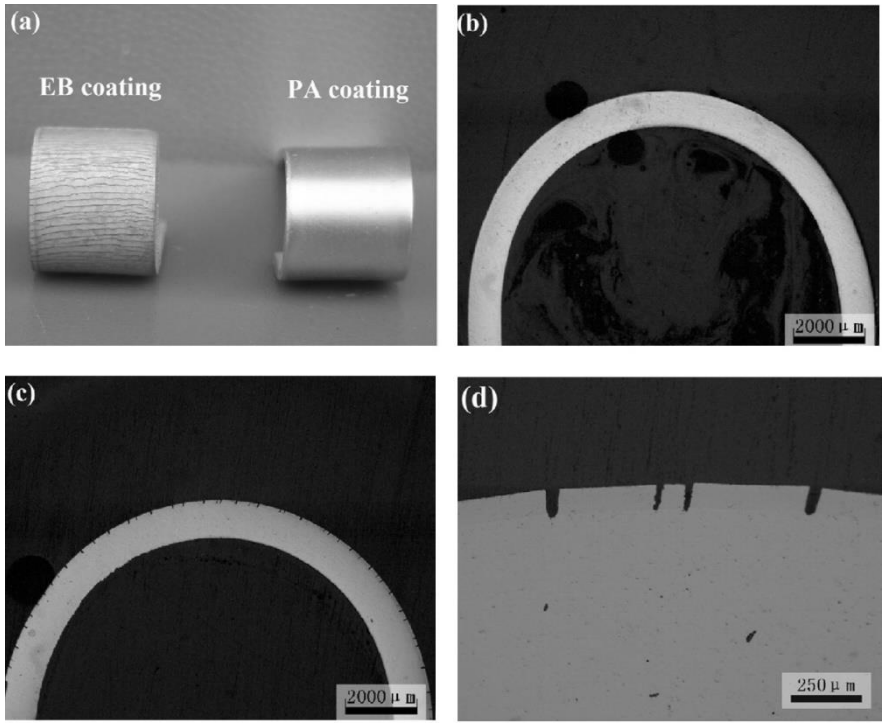

Figure 32. Analyzing the bending test outcomes: (a) photo micrographs of the surfaces and (b) cross sections for PA sample and (c, d) EB sample [115].

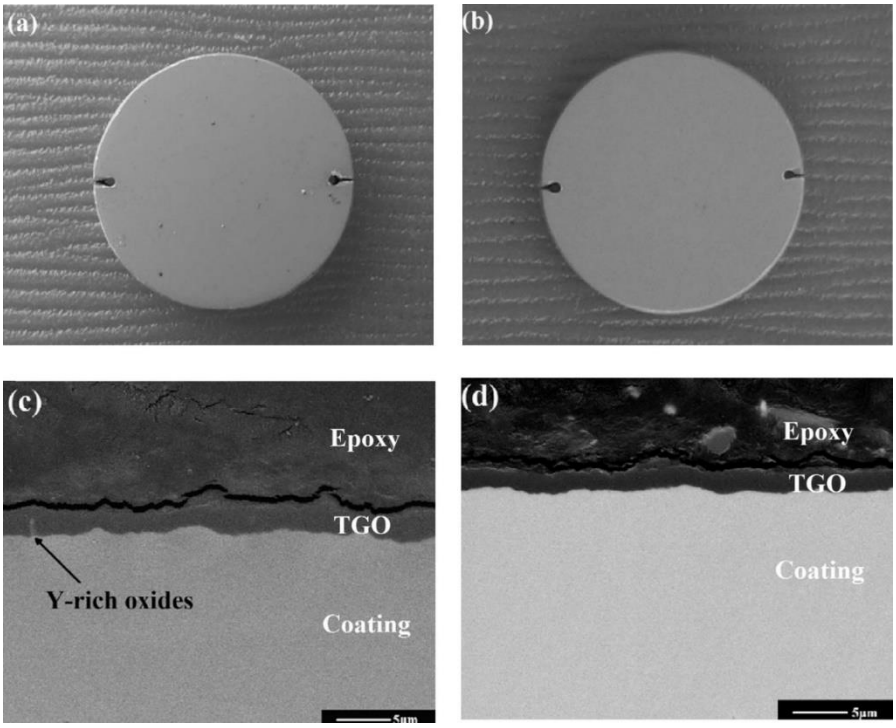

Figure 33. After 100 hours of oxidation, the coatings were imaged through photomicrographs of (a) EB and (b) PA sample surfaces, as well as (c) EB and (d) PA sample cross-sectional micrographs [115].

3.4.2. Thin gold protection radiation heat load in the system for cooling heat pipes

Research shows that the hydrogen heat pipeline (HHP) target cryogenic, which has a thin layer of gold coating, needs to be put through an external testing procedure before it can be used in the Cooler Synchrotron (COSY). With the aid of gravity, a gold-coated heating tube with a diameter of 5 mm was created and tested. This heat pipe's function is to speed up the cooling process of a hydrogen liquid target used in COSY's external beam tests. Research was conducted to ascertain the impact of reducing the heat pipe diameter from 7 to 5 mm in order to obtain a narrow target diameter. In order to reduce the radiation heat load, the effects of adding a polished gold layer to the heat pipe's outside surface as well as using a heat pipe without 20 layers of aluminum-coated mylar foil for super insulation were explored. Through testing, both with and without the use of 20 layers of superinsulation, the effectiveness of the gold-coated heat pipes was determined. In order to highlight the advantages and disadvantages of each situation, a comparison was made between their functioning characteristics. The heat pipe's efficiency was improved by lowering its surface emissivity, which was accomplished by covering its exterior with polished gold and reducing its diameter from 7 to 5 mm. As a result of this adjustment, both the heat load and the heat capacity decreased [116,117].

The duration of the cooling process, from the initiation of cooling until the LH_2 reaches the intended cell, is reduced from 48 to 44 minutes when superinsulation is not present. The equation for blackbody radiation can be employed for the purpose of quantifying the thermal radiation present in the surrounding environment.

One approach to decreasing the heat radiation load on the gas tube involves reducing its surface area from 177 to 38 cm^2. This can be accomplished by shortening the tube from 180 to 40 cm in length as illustrated in Figure 34. This modification also results in a reduction in the heat capacity of the tube. The emissivity of a gas tube can be reduced by subjecting it to high polishing prior to and subsequent to the application of a very thin gold coating [118].

Consequently, the enhancement of the liquefaction efficiency of gases can be attributed to the reduction in power dissipation. Table 7 displays the heat load resulting from blackbody radiation for a stainless-steel gas tube with a diameter of 0.3 cm and a length of 180 cm in the absence of gold coating and aluminum shielding. The heat load is reported to be 3.1 W for the entire length of the tube and 0.64 W for a length of 40 cm.

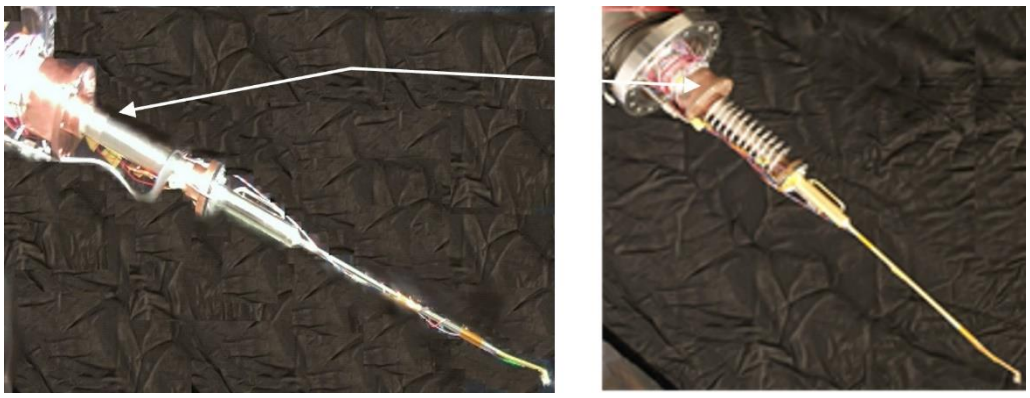

Figure 34. A gas tube of 0.3 cm diameter at lengths of (a) 40 cm and (b) 180 cm [118].

The primary aim of this study is to decrease the cool-down time of a heat pipe with specific characteristics, including a 7 mm diameter, a gold coating, and a shorter gas tube. Additionally, the cool-down time will be enhanced by a 10% increase for both liquid hydrogen (LH_2) and liquid deuterium (LD_2). Modifying the surface characteristics and dimensions of the gas tube can effectively decrease the heat radiation load on the target, thereby enhancing the cooling rate. Due to the gas tube's weight dropping from 38 to 13 g, the system's total heat capacity was reduced by a factor of three. A 40 cm short gas tube's heat burden decreased by a factor of 52 [119,120].

Table 7. Summarized the heat loads from radiation and conduction for the two gas tubes length [118].

Gas tube length (cm)	Radiation heat load on a non-isolated system (W)	Radiation heat load on an isolated system without gold coating (W)	Radiation heat load, isolated system with gold coating (W)	Conduction heat load (W)	Total heat load with gold coating (W)
180	3.1	2.39×10^{-3}	1.07×10^{-4}	1.01×10^{-6}	1.08×10^{-4}
40	0.642	5.50×10^{-4}	2.40×10^{-5}	2.03×10^{-5}	4.40×10^{-5}

4. Conclusion

This paper gives a thorough summary of the methods used today for surface modification in the field of engineering materials protection, with a focus on enhancing their mechanical and thermal characteristics. Researchers are particularly interested in the various applications of surface coatings, ion implantations and laser beam treatment.

These techniques offer benefits such as corrosion and wear resistance, thermal protection, reduced thermal load and improved hardness. The application of coating technology involves the addition of layers such as TiC, TiN, TiCN, SiVxN, TiB, CrN, TiAlN, TiAlON and TiAlC, with the aim of enhancing specific properties. For instance, in cutting tool applications, coating technology is utilized to increase the hardness and resistance to wear of the tool.

The characteristics of PVD-deposited films are influenced by a multitude of factors, including layer composition, monolayer and duplex structures, graded layers, multilayer configurations, reactive gas proportions and substrate temperature.

The utilization of ion implantation has emerged as a compelling method for the treatment of industrial tooling. Smooth surfaces and hard, multi-layered coatings exhibited superior wear resistance. The surface properties of materials can be enhanced through the process of ion implantation, which involves the introduction of ions such as nitrogen, carbon or boron under varying conditions.

The enhancement of the lifespan of parts exposed to high temperatures can be achieved by incorporating protective layers, as proposed by TBC.

Thermal barrier coatings' (TBCs') long-term durability is impacted by the thermally grown oxide (TGO) between the ceramic and bond coat at elevated temperatures. One of the primary factors contributing to the failure of interdiffusion that takes place inside the bond coat and at the bond coat and substrate interface is a characteristic of thermal barrier coatings (TBCs).

When compared to layers produced using physical vapor deposition using an electron beam (EB-PVD), layers deposited using plasma-assisted electron beam deposition (PA-EBPVD) have better properties.

Laser-based methodologies were found to improve the surface characteristics of engineering materials, including but not limited to hardness, wear resistance and surface roughness. These improvements can be achieved through a variety of techniques, whether applied to bulk materials or coated layers.

Plasma electrolytic oxidation (PEO) coatings exhibit enhanced thermal, mechanical, and corrosion properties.

Peening techniques are crucial for enhancing strength against fatigue by reducing crack growth. These techniques have the ability to optimize stress distribution on the surface of a component while limiting deformation. Additionally, they can induce deeper residual compressive stresses in the layers and refine the microstructure of the strained surface layer. These advancements make peening techniques highly promising for various significant applications in engineering in the foreseeable future.

Enhancing the operational efficiency of heat pipes utilized in low-temperature COSY targets can be achieved by using a gold coating that is applied in a thin layer.

Use of AI tools declaration

The authors declare they have not used artificial intelligence (AI) tools in the creation of this article.

Conflict of interest

The author declares no conflict of interest.

References

1. Barshilia HC, Selvakumar N, Rajam KS, et al. (2008) Deposition and characterization of TiAlN/TiAlON/Si_3N_4 tandem absorbers prepared using reactive direct current magnetron sputtering. *Thin Solid Films* 516: 6071–6078. https://doi.org/10.1016/j.tsf.2007.10.113
2. Matthews A, Rickerby DS (1991) *Advanced Surface Coatings: A Handbook of Surface Engineering*, New York: Springer Dordrecht.
3. Setiawan T, Abidin Z, Hendra C (2021) Making prototype of electro plating equipment for home industryome industri. *JITTER* 8: 145–149. https://doi.org/10.33197/jitter.vol8.iss1.2021.735
4. Prathap P, Riyaz SM, Sai GM, et al. (2020) Experimental investigation of chromium and nickel thin sheets on EN8 steel by plating technique. *IJSRED* 4: 509–516. Available from: www.ijsred.com/volume3/issue2/IJSRED-V3I2P77.pdf.
5. Zhang WH, Fei JY, Luo LL, et al. (2013) High speed pulse electro plating process of nickel. *J Chin Soc Corros Prot* 33: 317–324. https://www.jcscp.org/EN/Y2013/V33/I4/317
6. Choquette Y, Menard H, Brossard L (1990) Electrocatalytic performance of composite-coated electrodes for alkaline water electrolysis. *Int J Hydrogen Energy* 15: 21–26. https://doi.org/10.1016/0360-3199(90)90126-J
7. Bunshah RF, Weissmantel C (2001) *Handbook of Hard Coatings: Deposition Technologies, Properties and Applications*, Park Ridge NJ: Noyes Publications.

8. Dogan H, Findik F, Morgul O (2002) Friction and wear behaviour of implanted AISI 316L SS and comparison with a substrate. *Mater Design* 23: 605–610. https://doi.org/10.1016/S0261-3069(02)00066-3
9. El-Awadi GA, Abdel-Samad S, Waheed AF (2013) Characterization and properties of TiAlC layer on hard metal substrate WC/Co deposited by physical vapor deposition. *Arab J Nucl Sci Appl* 46: 195–202.
10. Dogan H, Findik F, Morgul O (2002) Friction and wear behaviour of implanted AISI 316L SS and comparison with a substrate. *Mater Design* 23: 605–610. https://doi.org/10.1016/S0261-3069(02)00066-3
11. Creighton JR, Ho P (2001) Introduction to chemical vapor deposition (CVD), In: Xu YD, Yan XT, *Chemical Vapour Deposition*, London: Springer London.
12. Selvakumar N, Barshilia HC (2012) Review of physical vapor deposited (PVD) spectrally selective coatings for mid-and high-temperature solar thermal applications. *Sol Energ Mat Sol C* 98: 1–23. https://doi.org/10.1016/j.solmat.2011.10.028
13. Popok V, Campbell EEB (2006) Beams of atomic clusters: Effects on impact with solids. *Rev Adv Mater Sci* 11: 19–45.
14. Stappen MV, Stals LM, Kerkhofs M, et al. (1995) State of the art for the industrial use of ceramic PVD coatings. *Surf Coat Tech* 74–75: 629–633. https://doi.org/10.1016/0257-8972(95)08296-4
15. Azam RM (2017) *The Study of Chromium Nitride Coating by Asymmetric Bipolar Pulsed DC Reactive Magnetron Sputtering*, Lappeenranta: Lappeenranta University of Technology.
16. Thilakan P, Minarini C, Loreti S, et al. (2001) Investigations on the crystallisation properties of RF magnetron sputtered indium tin oxide thin films. *Thin Solid Films* 388: 34–40. https://doi.org/10.1016/S0040-6090(01)00820-3
17. Freller H, Haessler H (1988) Evaluation of existing ion plating processes for the deposition of multicomponent hard coatings. *Surf Coat Tech* 36: 219–232. https://doi.org/10.1016/0257-8972(88)90152-1
18. Ko J, Kim JW, Min HW, et al. (2022) Review of manufacturing technologies for coated accident tolerant fuel cladding. *J Nucl Mater* 561: 153562. https://doi.org/10.1016/j.jnucmat.2022.153562
19. Bouzakis KD, Michailidis N, Skordaris G, et al. (2012) Cutting with coated tools: Coating technologies, characterization methods and performance optimization. *CIRP Ann* 61: 703–723. https://doi.org/10.1016/j.cirp.2012.05.006
20. Soum-Glaude A, Le Gal A, Bichotte M, et al. (2017) Optical characterization of $TiAlN_x/TiAlN_y/Al_2O_3$ tandem solar selective absorber coatings. *Sol Energ Mat Sol C* 170: 254–262. https://doi.org/10.1016/j.solmat.2017.06.007
21. Rudnev V, Loveless D, Cook RL (2017) *Handbook of Induction Heating*, Boca Raton: CRC press.
22. Heimann RB (2008) *Plasma-Spray Coating: Principles and Applications*, Weinheim: John Wiley & Sons.
23. Herman H, Sampath S, McCune R (2000) Thermal spray: Current status and future trends. *MRS Bull* 25: 17–25. https://doi.org/10.1557/mrs2000.119
24. Deshpande S, Sampath S, Zhang H (2006) Mechanisms of oxidation and its role in microstructural evolution of metallic thermal spray coatings—Case study for Ni–Al. *Surf Coat Tech* 200: 5395–5406. https://doi.org/10.1016/j.surfcoat.2005.07.072

25. Jordan EH, Jiang C, Gell M (2015) The solution precursor plasma spray (SPPS) process: A review with energy considerations. *J Therm Spray Techn* 24: 1153–1165. https://doi.org/10.1007/s11666-015-0272-9
26. Jansson U, Lewin E, Rasander M, et al. (2011) Design of carbide-based nanocomposite thin films by selective alloying. *Surf Coat Tech* 206: 583–590. https://doi.org/10.1016/j.surfcoat.2010.06.017
27. Strnad G, Buhagiar J (2010) Latest developments in PVD coatings for tooling. *AMSET* 7: 32–37.
28. Fuentes GG (2010) Surface engineering and micro-manufacturing, In: Qin Y, *Micromanufacturing Engineering and Technology*, Boston: William Andrew Publishing.
29. Harris SG, Doyle ED, Wong YC, et al. (2004) Reducing the macroparticle content of cathodic arc evaporated TiN coatings. *Surf Coat Tech* 183: 283–294. https://doi.org/10.1016/j.surfcoat.2003.08.086
30. Jansson U, Lewin E (2013) Sputter deposition of transition-metal carbide films—A critical review from a chemical perspective. *Thin Solid Films* 536: 1–24. https://doi.org/10.1016/j.tsf.2013.02.019
31. Hoche H, Groß S, Oechsner M (2014) Development of new PVD coatings for magnesium alloys with improved corrosion properties. *Surf Coat Tech* 259: 102–108. https://doi.org/10.1016/j.surfcoat.2014.04.038
32. Kuroda S (1998) Properties and characterization of thermal sprayed coatings and a review of recent research progress. *ITSC* 1998: 539–550. https://doi.org/10.31399/asm.cp.itsc1998p0539
33. Ang ASM, Sanpo N, Sesso ML, et al. (2013) Thermal spray maps: Material genomics of processing technologies. *J Therm Spray Techn* 22: 1170–1183. https://doi.org/10.1007/s11666-013-9970-3
34. Vetter J, Barbezat G, Crummenauer J, et al. (2005) Surface treatment selections for automotive applications. *Surf Coat Tech* 200: 1962–1968. https://doi.org/10.1016/j.surfcoat.2005.08.011
35. Jagadeeshanayaka N, Awasthi S, Jambagi SC, et al. (2022) Bioactive surface modifications through thermally sprayed hydroxyapatite composite coatings: A review over selective reinforcements. *Biomate Sci* 10: 2484–2523. https://doi.org/10.1039/D2BM00039C
36. Amanov A (2019) Wear resistance and adhesive failure of thermal spray ceramic coatings deposited onto graphite in response to ultrasonic nanocrystal surface modification technique. *Appl Surf Sci* 477: 184–197. https://doi.org/10.1016/j.apsusc.2017.11.013
37. Fu Y, Wei J, Batchelor AW (2000) Some considerations on the mitigation of fretting damage by the application of surface-modification technologies. *J Mater Process Tech* 99: 231–245. https://doi.org/10.1016/S0924-0136(99)00429-X
38. Guemmaz M, Mosser A, Grob JJ, et al. (1996) Composition and structure of titanium carbonitride thin film synthesized by ion implantation. *Surf Coat Tech* 80: 53–56. https://doi.org/10.1016/0257-8972(95)02684-3
39. Dong H, Bell T (1999) State-of-the-art overview: Ion beam surface modification of polymers towards improving tribological properties. *Surf Coat Tech* 111: 29–40. https://doi.org/10.1016/S0257-8972(98)00698-7
40. Sharma MK, Jang Y, Kim J, et al. (2014) Plasma electrolytic oxidation in surface modification of metals for electronics. *JWJ* 32: 241–247. https://doi.org/10.5781/JWJ.2014.32.3.27

41. Simchen F, Sieber M, Kopp A, et al. (2020) Introduction to plasma electrolytic oxidation—An overview of the process and applications. *Coatings* 10: 628. https://doi.org/10.3390/coatings10070628
42. Makurat-Kasprolewicz B, Ossowska A (2023) Recent advances in electrochemically surface treated titanium and its alloys for biomedical applications: A review of anodic and plasma electrolytic oxidation methods. *Mater Today Commun* 34: 105425. https://doi.org/10.1016/j.mtcomm.2023.105425
43. Sikdar S, Menezes PV, Maccione R, et al. (2021) Plasma electrolytic oxidation (PEO) process—Processing, properties, and applications. *Nanomaterials* 11: 1375. https://doi.org/10.3390/nano11061375
44. Abdulla T (2013) *The Effect of Pulsed Bipolar Plasma Electrolytic Oxidation Coatings on the Mechanical Properties of Open Cell Aluminium Foams*, Sheffield: University of Sheffield.
45. Kaseem M, Fatimah S, Nashrah N, et al. (2021) Recent progress in surface modification of metals coated by plasma electrolytic oxidation: Principle, structure, and performance. *Prog Mater Sci* 117: 100735. https://doi.org/10.1016/j.pmatsci.2020.100735
46. Walsh FC, Low CTJ, Wood RJK, et al. (2009) Plasma electrolytic oxidation (PEO) for production of anodised coatings on lightweight metal (Al, Mg, Ti) alloys. *Trans IMF* 87: 122–135. https://www.tandfonline.com/doi/abs/10.1179/174591908X372482
47. Kaseem M, Choe HC (2021) Simultaneous improvement of corrosion resistance and bioactivity of a titanium alloy via wet and dry plasma treatments. *J Alloy Compd* 851: 156840. https://doi.org/10.1016/j.jallcom.2020.156840
48. Kaseem M, Hussain T, Rehman ZU, et al. (2021) Stabilization of AZ31 Mg alloy in sea water via dual incorporation of MgO and WO_3 during micro-arc oxidation. *J Alloy Compd* 853: 157036. https://doi.org/10.1016/j.jallcom.2020.157036
49. Hussain T, Kaseem M, Ko YG (2020) Hard acid–hard base interactions responsible for densification of alumina layer for superior electrochemical performance. *Corros Sci* 170: 108663. https://doi.org/10.1016/j.corsci.2020.108663
50. Kaseem M, Hussain T, Zeeshan UR, et al. (2021) Fabrication of functionalized coating with a unique flowery-flake structure for an effective corrosion performance and catalytic degradation. *Chem Eng J* 420: 129737. https://doi.org/10.1016/j.cej.2021.129737
51. Kim SP, Kaseem M, Choe HC (2020) Plasma electrolytic oxidation of Ti-25Nb-xTa alloys in solution containing Ca and P ions. *Surf Coat Technol* 395: 125916. https://doi.org/10.1016/j.surfcoat.2020.125916
52. Qutaba S, Asmelash M, Saptaji K, et al. (2022) A review on peening processes and its effect on surfaces. *Int J Adv Manuf Technol* 120: 4233–4270. https://doi.org/10.1007/s00170-022-09021-6
53. Ye C, Zhang C, Zhao J, et al. (2021) Effects of post-processing on the surface finish, porosity, residual stresses, and fatigue performance of additive manufactured metals: A review. *J Mater Eng Perform* 30: 6407–6425. https://doi.org/10.1007/s11665-021-06021-7
54. Clauer AH (1996) Laser shock peening for fatigue resistance, In: Gregory JK, Rack HJ, Eylon D, *Surface Performance of Titanium*, Warrendale: The Metal Society of AIME.
55. Ding K, Ye L (2006) *Laser Shock Peening: Performance and Process Simulation*, Cambridge: Woodhead Publishing.

56. Sanchez AG, You C, Leering M, et al. (2021) Effects of laser shock peening on the mechanisms of fatigue short crack initiation and propagation of AA7075-T651. *Int J Fatigue* 143: 106025. https://doi.org/10.1016/j.ijfatigue.2020.106025
57. Achintha M, Nowell D, Fufari D, et al. (2014) Fatigue behaviour of geometric features subjected to laser shock peening: Experiments and modelling. *Int J Fatigue* 62: 171–179. https://doi.org/10.1016/j.ijfatigue.2013.04.016
58. Sticchi M, Schnubel D, Kashaev N, et al. (2015) Review of residual stress modification techniques for extending the fatigue life of metallic aircraft components. *Appl Mech Rev* 67: 010801. https://doi.org/10.1115/1.4028160
59. Maharjan N, Chan SY, Ramesh T, et al. (2021) Fatigue performance of laser shock peened Ti6Al4V and Al6061-T6 alloys. *Fatigue Fract Eng M* 44: 733–747. https://doi.org/10.1111/ffe.13390
60. Torkaman H (2018) Modeling and analysis of the shot peening process: A study of the residual stresses in an insert using the finite element method. Available from: https://lnu.diva-portal.org/smash/get/diva2:1241705/FULLTEXT02.pdf.
61. Spadaro L, Hereñú S, Strubbia R, et al. (2020) Effects of laser shock processing and shot peening on 253 MA austenitic stainless steel and their consequences on fatigue properties. *Opt Laser Technol* 122: 105892. https://doi.org/10.1016/j.optlastec.2019.105892
62. Qutaba S, Asmelash M, Saptaji K, et al. (2022) A review on peening processes and its effect on surfaces. *Int J Adv Manuf Technol* 120: 4233–4270. https://doi.org/10.1007/s00170-022-09021-6
63. Van Aswegen DC, Polese C (2021) Experimental and analytical investigation of the effects of laser shock peening processing strategy on fatigue crack growth in thin 2024 aluminium alloy panels. *Int J Fatigue* 142: 105969. https://doi.org/10.1016/j.ijfatigue.2020.105969
64. Zhang X, Yang M, Zhou C, et al. (2022) A comprehensive review of fatigue behavior of laser shock peened metallic materials. *Theor Appl Fract Mech* 122: 103642. https://doi.org/10.1016/j.tafmec.2022.103642
65. Li G, Dong Z, Luo T, et al. (2023) Study on the influence of shot peening strengthening before shot peen forming on 2024-T351 aluminum alloy fatigue crack growth rate. *Sci Rep* 13: 5313. https://doi.org/10.1038/s41598-023-32616-2
66. Wang H, Ning C, Huang Y, et al. (2017) Improvement of abrasion resistance in artificial seawater and corrosion resistance in NaCl solution of 7075 aluminum alloy processed by laser shock peening. *Opt Laser Eng* 90: 179–185. https://doi.org/10.1016/j.optlaseng.2016.10.016
67. Tan Y, Wu G, Yang JM, et al. (2004) Laser shock peening on fatigue crack growth behaviour of aluminium alloy. *Fatigue Fract Eng M* 27: 649–656. https://doi.org/10.1111/j.1460-2695.2004.00763.x
68. Vorbau M, Hillemann L, Stintz M (2009) Method for the characterization of the abrasion induced nanoparticle release into air from surface coatings. *J Aerosol Sci* 40: 209–217. https://doi.org/10.1016/j.jaerosci.2008.10.006
69. Baer DR, Thevuthasan S (2010) Characterization of thin films and coatings, In: Martin PM, *Handbook of Deposition Technologies for Films and Coatings*, Boston: William Andrew Publishing.
70. Tkadletz M, Schalk N, Daniel R, et al. (2016) Advanced characterization methods for wear resistant hard coatings: A review on recent progress. *Surf Coat Technol* 285: 31–46. https://doi.org/10.1016/j.surfcoat.2015.11.016

71. Wolke JGC, van Dijk K, Schaeken HG, et al. (1994) Study of the surface characteristics of magnetron-sputter calcium phosphate coatings. *J Biomed Mater Res* 28: 1477–1484. https://doi.org/10.1002/jbm.820281213
72. Benmalek M, Gimenez P, Peyre JP, et al. (1991) Characterization and comparison of TiN layers deposited by different physical vapour deposition processes. *Surf Coat Technol* 48: 181–187. https://doi.org/10.1016/0257-8972(91)90001-D
73. Dearnaley G, Arps J (2006) Ion surface treatment of materials, In: Pauleau Y, *Materials Surface Processing by Directed Energy Techniques*, Oxford: Elsevier.
74. Ahmed MS (2013) Effect of thermal annealing and carbon implantation on the functional properties of nanocomposite TiSiN coatings on steel. Available from: https://ro.ecu.edu.au/theses/536.
75. Zu XT, Wang ZG, Feng XD, et al. (2003) Surface characterization of a Ti-2Al-2.5Zr alloy by nitrogen ion implantation. *J Alloy Compd* 351: 114–118. https://doi.org/10.1016/S0925-8388(02)01094-0
76. Takano I, Isobe S, Sasaki TA, et al. (1989) Nitrogenation of various transition metals by N_2^+-ion implantation. *Appl Surf Sci* 37: 25–32. https://doi.org/10.1016/0169-4332(89)90970-7
77. Gevorkyan E, Rucki M, Nerubatskyi VP, et al. (2022) *Remanufacturing and Advanced Machining Processes for New Materials and Components*, London: Taylor & Francis.
78. Hartley NEW (1975) Ion implantation and surface modification in tribology. *Wear* 34: 427–438. https://doi.org/10.1016/0043-1648(75)90109-X
79. König U, Wolf GK (1987) Effects of ion implantation in cemented carbides and cobalt alloys. *Surf Coat Technol* 33: 501–509. https://doi.org/10.1016/0257-8972(87)90214-3
80. Lu T, Qiao Y, Liu X (2012) Surface modification of biomaterials using plasma immersion ion implantation and deposition. *Interface Focus* 2: 325–336. https://doi.org/10.1098/rsfs.2012.0003
81. Belbah A, Mkaddem A, Ladaci N, et al. (2014) Low energy implantation to inhibit wear in N^+ ions implanted WC-Co composite. *Mater Design* 53: 202–208. https://doi.org/10.1016/j.matdes.2013.07.014
82. Rapoport L, Moshkovich A, Perfilyev V, et al. (2014) High temperature friction behavior of CrV_xN coatings. *Surf Coat Technol* 238: 207–215. https://doi.org/10.1016/j.surfcoat.2013.10.076
83. Rapoport L, Moshkovich A, Perfilyev V, et al. High temperature friction behavior of CrV_xN coatings. *Surf Coat Technol* 238: 207–215.https://doi.org/10.1016/j.surfcoat.2013.10.076
84. Li Y, Liu Z, Luo J, et al. (2019) Microstructure, mechanical and adhesive properties of CrN/CrTiAlSiN/WCrTiAlN multilayer coatings deposited on nitrided AISI 4140 steel. *Mater Charact* 147: 353–364. https://doi.org/10.1016/j.matchar.2018.11.017
85. Liew WYH, Lim HP, Melvin GJH, et al. (2022) Thermal stability, mechanical properties, and tribological performance of TiAlXN coatings: Understanding the effects of alloying additions. *J Mater Res Technol* 17: 961–1012. https://doi.org/10.1016/j.jmrt.2022.01.005
86. Chang YY, Chao LC (2021) Effect of substrate bias voltage on the mechanical properties of AlTiN/CrTiSiN multilayer hard coatings. *Vacuum* 190: 110241. https://doi.org/10.1016/j.vacuum.2021.110241
87. Keunecke M, Stein C, Bewilogua K, et al. (2010) Modified TiAlN coatings prepared by dc pulsed magnetron sputtering. *Surf Coat Technol* 205: 1273–1278. https://doi.org/10.1016/j.surfcoat.2010.09.023

88. Yan H, Tian Q, Gao D, et al. (2019) Microstructure and properties of TiAlN/AlN multilayers with different modulation periods. *Surf Coat Technol* 363: 61–65. https://doi.org/10.1016/j.surfcoat.2019.01.064
89. Kern KT, Walter KC, Griffin Jr AJ, et al. (1997) Boron and nitrogen implantation of steels. *Nucl Instrum Meth B* 127–128: 972–976. https://doi.org/10.1016/S0168-583X(97)00041-4
90. Brown IG, Godechot X, Yu KM (1991) Novel metal ion surface modification technique. *Appl Phys Lett* 58: 1392–1394. https://doi.org/10.1063/1.104318
91. Conrad JR, Dodd RA, Han S, et al. (1990) Ion beam assisted coating and surface modification with plasma source ion implantation. *J Vac Sci Technol A* 8: 3146–3151. https://doi.org/10.1116/1.576598
92. Kurella A, Dahotre NB (2005) Surface modification for bioimplants: The role of laser surface engineering. *J Biomater Appl* 20: 5–50. https://doi.org/10.1177/0885328205052974
93. Brown MS, Arnold CB (2010) Fundamentals of laser-material interaction and application to multiscale surface modification, In: Sugioka K, Meunier M, Piqué A, *Laser Precision Microfabrication*, Heidelberg: Springer.
94. Tian YS, Chen CZ, Li ST, et al. (2005) Research progress on laser surface modification of titanium alloys. *Appl Surf Sci* 242: 177–184. https://doi.org/10.1016/j.apsusc.2004.08.011
95. Chikarakara E, Naher S, Brabazon D (2012) High speed laser surface modification of Ti-6Al-4V. *Surf Coat Technol* 206: 3223–3229. https://doi.org/10.1016/j.surfcoat.2012.01.010
96. De Damborenea J (1998) Surface modification of metals by high power lasers. *Surf Coat Technol* 100–101: 377–382. https://doi.org/10.1016/S0257-8972(97)00652-X
97. Ahmadi-Pidani R, Shoja-Razavi R, Mozafarinia R, et al. (2013) Laser surface modification of plasma sprayed CYSZ thermal barrier coatings. *Ceram Int* 39: 2473–2480. https://doi.org/10.1016/j.ceramint.2012.09.005
98. Krishnan R, Dash S, Kesavamoorthy R, et al. (2006) Laser surface modification and characterization of air plasma sprayed alumina coatings. *Surf Coat Technol* 200: 2791–2799. https://doi.org/10.1016/j.surfcoat.2005.05.002
99. Elambasseril J, Rogers J, Wallbrink C, et al. (2022) Laser powder bed fusion additive manufacturing (LPBF-AM): The influence of design features and LPBF variables on surface topography and effect on fatigue properties. *Crit Rev Solid State* 48: 132–168. https://doi.org/10.1080/10408436.2022.2041396
100. Mallikarjuna (2020) *Effect of Process Variables on Residual Stress and Microstructure in Laser Additive Manufacturing of γ-TiAl Alloy*, Surathkal: National Institute of Technology Karnataka.
101. Zhou YC, Yang L, Zhu W (2022) *Thermal Barrier Coatings: Failure Theory and Evaluation Technology*, Singapore: Springer.
102. Bennett A (1986) Properties of thermal barrier coatings. *Mater Sci Technol* 2: 257–261. https://doi.org/10.1179/mst.1986.2.3.257
103. Zhou F, Wang Y, Wang L, et al. (2017) High temperature oxidation and insulation behavior of plasma-sprayed nanostructured thermal barrier coatings. *J Alloy Compd* 704: 614–623. https://doi.org/10.1016/j.jallcom.2017.02.073
104. Mehta A, Vasudev H, Singh S, et al. (2022) Processing and advancements in the development of thermal barrier coatings: A review. *Coatings* 12: 1318. https://doi.org/10.3390/coatings12091318

105. Beele W, Marijnissen G, Van Lieshout A (1999) The evolution of thermal barrier coatings—status and upcoming solutions for today's key issues. *Surf Coat Technol* 120: 61–67. https://doi.org/10.1016/S0257-8972(99)00342-4
106. Padture NP, Gell M, Jordan EH (2002) Thermal barrier coatings for gas-turbine engine applications. *Science* 296: 280–284. https://doi.org/10.1126/science.1068609
107. Yao Z, Hu K, Li R (2019) Enhanced high-temperature thermal fatigue property of aluminum alloy piston with Nano PYSZ thermal barrier coatings. *J Alloy Compd* 790: 466–479. https://doi.org/10.1016/j.jallcom.2019.03.177
108. Caputo S, Millo F, Boccardo G, et al. (2019) Numerical and experimental investigation of a piston thermal barrier coating for an automotive diesel engine application. *Appl Therm Eng* 162: 114233. https://doi.org/10.1016/j.applthermaleng.2019.114233
109. Akhtar AF, Yadav D (2022) Review paper on simulation, analysis and validation on thermal barrier coated piston of diesel engine. *Int Res J Mod Eng Technol Sci* 4: 1478–1490.
110. Mahade S, Curry N, Björklund S, et al. (2015) Thermal conductivity and thermal cyclic fatigue of multilayered $Gd_2Zr_2O_7$/YSZ thermal barrier coatings processed by suspension plasma spray. *Surf Coat Technol* 283: 329–336. https://doi.org/10.1016/j.surfcoat.2015.11.009
111. Mahade S, Curry N, Björklund S, et al. (2017) Functional performance of $Gd_2Zr_2O_7$/YSZ multi-layered thermal barrier coatings deposited by suspension plasma spray. *Surf Coat Technol* 318: 208–216. https://doi.org/10.1016/j.surfcoat.2016.12.062
112. Mahade S, Curry N, Jonnalagadda KP, et al. (2019) Influence of YSZ layer thickness on the durability of gadolinium zirconate/YSZ double-layered thermal barrier coatings produced by suspension plasma spray. *Surf Coat Technol* 357: 456–465. https://doi.org/10.1016/j.surfcoat.2018.10.046
113. Leng K, Romero AR, Venturi F, et al. (2022) Solution precursor thermal spraying of gadolinium zirconate for thermal barrier coating. *J Eur Ceram Soc* 42: 1594–1607. https://doi.org/10.1016/j.jeurceramsoc.2021.11.050
114. Mondal K, Nuñez Iii L, Downey CM, et al. (2021) Thermal barrier coatings overview: Design, manufacturing, and applications in high-temperature industries. *Ind Eng Chem Res* 60: 6061–6077. https://doi.org/10.1021/acs.iecr.1c00788
115. He J, Guo H, Peng H, et al. (2013) Microstructural, mechanical and oxidation features of NiCoCrAlY coating produced by plasma activated EB-PVD. *Appl Surf Sci* 274: 144–150. https://doi.org/10.1016/j.apsusc.2013.02.136
116. Guo Y, Lin G, Zhang H, et al. (2018) Investigation on thermal behaviours of a methane charged cryogenic loop heat pipe. *Energy* 157: 516–525. https://doi.org/10.1016/j.energy.2018.05.133
117. Abdel-Samad S, Abdel-Bary M, Kilian K (2002) New developments in cryo-targets for the external COSY experiments. *Nucl Instrum Meth A* 495: 1–7. https://doi.org/10.1016/S0168-9002(02)01561-9
118. Abdel-Bary M, Abdel-Samad S, Kilian K (2005) A very light and thin liquid hydrogen/deuterium heat pipe target for COSY experiments. *Cryogenics* 45: 489–495. https://doi.org/10.1016/j.cryogenics.2005.05.001
119. Abdel-Bary M, Abdel-Samad S, Elawadi GA, et al. (2009) A thin gold coated hydrogen heat pipe-cryogenic target for external experiments at COSY. *Cryogenics* 49: 192–197. https://doi.org/10.1016/j.cryogenics.2009.01.003

120. El-Awadi GA, Abdel-Samad S, Abdel-Bary M, et al. (2009) Improving the performance of the cryogenic heat pipe-target system for the COSY-TOF experiment. *Vacuum* 83: 1321–1325. https://doi.org/10.1016/j.vacuum.2009.04.039